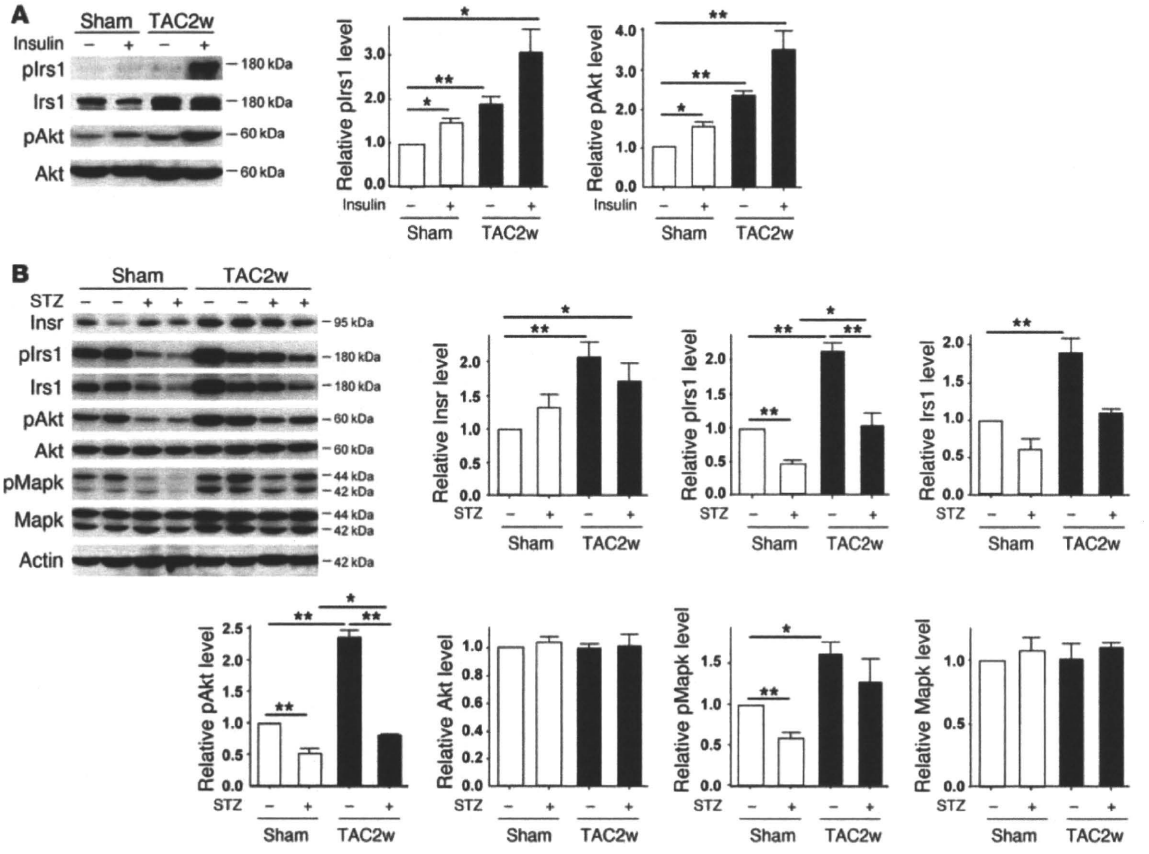

Figure 1

Upregulation of cardiac insulin signals by pressure overload. (**A**) Mice were subjected to TAC or sham operation (sham), and heart samples were obtained 2 weeks later. Mice were starved for 6 hours, and insulin or PBS was injected before sacrifice. pIrs1 and pAkt levels in the heart were examined by Western blot analysis. The graphs indicate relative expression levels of pIrs1 and pAkt. $n = 3$. TAC2w, 2 weeks after TAC. (**B**) Mice were subjected to TAC or sham operation and were sacrificed 2 weeks later. Components of the insulin signaling pathway in the heart were examined by Western blot analysis. The graphs indicate relative expression levels of these signaling molecules. $n = 3$. Data are shown as mean ± SEM. $^*P < 0.05$; $^{**}P < 0.01$.

myocardial hypoxia and cardiomyocyte death, leading to cardiac dysfunction (15). Moreover, intensive glycemic control of diabetic patients by insulin treatment has been reported to increase cardiovascular events (16). In the present study, we examined the role of insulin signaling in the development of cardiac dysfunction induced by pressure overload.

Results

Cardiac insulin signaling is activated by pressure overload. To investigate the role of the insulin signal pathway in failing hearts, we created severe transverse aortic constriction (TAC) in mice at 11 weeks of age. In this model, cardiac hypertrophy gradually progressed and reached a peak on day 7 after TAC (Supplemental Figure 1; supplemental material available online with this article; doi:10.1172/JCI40096DS1). Systolic function was preserved until day 7 but was significantly decreased on day 14 along with left ventricular dilatation (Supplemental Figure 1). Seven and fourteen days after TAC, we treated the mice with insulin (1 IU/kg) before sacrifice and examined the downstream signaling pathway of the insulin receptor (Insr) in the heart. Insulin-induced phosphorylation of insulin receptor substrate-1 (pIrs1) and Akt (pAkt) was markedly upregulated in the hearts of the TAC group compared with the sham-operated group (Figure 1A and Supplemental Figure 2A). We also found that the insulin signal pathway was constitutively activated in the TAC hearts under fasting conditions (Figure 1B and Supplemental Figure 2B). Expression of Insr and Irs1 protein as well as pIrs1 and pAkt protein was significantly increased in the TAC heart. These results suggest that chronic pressure overload upregulates cardiac insulin signaling. Enhanced insulin signaling was also observed in the hearts of spontaneously hypertensive rats (Supplemental Figure 3A).

Reduction of plasma insulin ameliorates systolic dysfunction induced by pressure overload. To determine whether upregulation of cardiac insulin signals has a pathological role in HF, we treated the mice with streptozotocin (STZ) (50 mg/kg i.p. for 5 days) at 4 weeks before TAC. Injection of STZ markedly decreased plasma insulin to below detectable levels, while the plasma glucose level gradually increased (Supplemental Figure 4). Pressure overload led to prominent cardiac hypertrophy along with upregulation of cardiac insulin signaling (Figure 1B and Figure 2, A and B). Systolic function was impaired and the left ventricular systolic dimension

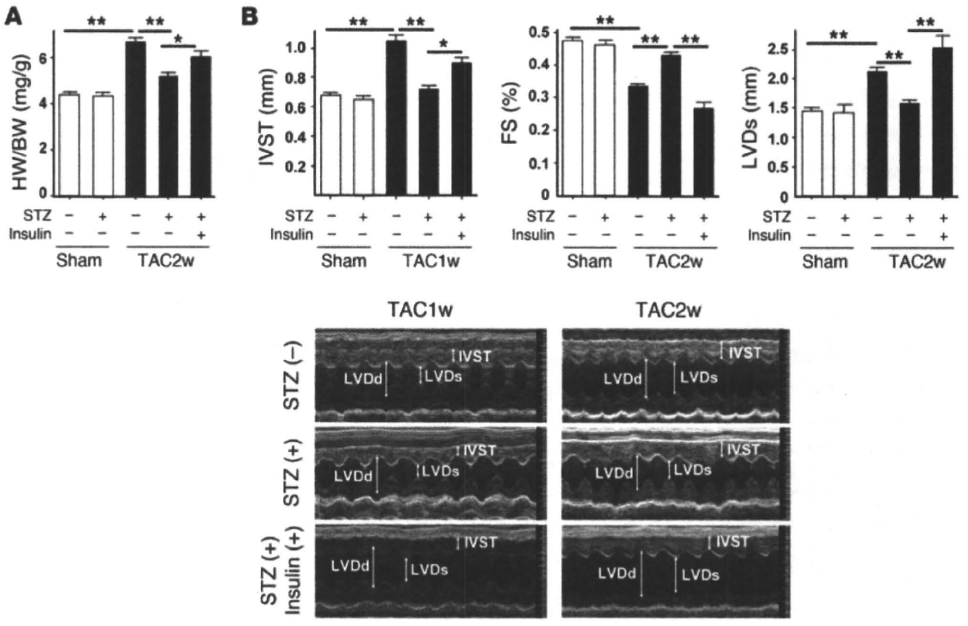

Figure 2

Depletion of plasma insulin attenuates systolic dysfunction induced by pressure overload. (**A**) STZ- or vehicle-treated mice were subjected to TAC or sham operation. The heart weight/body weight (HW/BW) ratio was measured 2 weeks after operation. In the insulin-treated group, daily i.p. injection of insulin (0.1 IU/g/d) was performed from 9 weeks (2 weeks after STZ treatment) to 13 weeks of age (2 weeks after TAC). n = 22–24. (**B**) Cardiac hypertrophy and systolic function of the animals prepared for **A** were estimated by echocardiography at 1 week (IVST) or 2 weeks (FS and LVDs) after operation. Photographs show representative results of echocardiography (M-mode). n = 6–10. Data are shown as mean ± SEM. $^*P < 0.05$; $^{**}P < 0.01$. IVST, intraventricular septal thickness; FS, fractional shortening.

(LVDs) was increased at 14 days after TAC (Figure 2, A and B). These alterations were significantly ameliorated in the mice treated with STZ (Figure 1B and Figure 2, A and B). Similar results were obtained at 6 weeks after TAC (Supplemental Figure 2C). We next examined the effect of insulin on cardiac function in this setting. STZ-treated mice were subjected to daily injection of insulin (0.1 IU/g/d from 9 weeks to 13 weeks of age) and to TAC at 11 weeks of age. Insulin treatment significantly improved hyperglycemia (Supplemental Figure 4). However, this treatment significantly enhanced cardiac hypertrophy and decreased systolic function along with left ventricular dilatation (Figure 2, A and B), indicating that insulin signaling influenced the development of systolic dysfunction due to pressure overload.

Reduction of plasma insulin inhibits cardiac hypoxia during pressure overload. We have recently demonstrated that cardiac angiogenesis is critically involved in the adaptive mechanism of cardiac hypertrophy and that an increased mismatch between cardiomyocyte size and vascularity is a crucial determinant of the transition from cardiac hypertrophy to HF (15). Consistent with our previous results, chronic pressure overload increased the cross-sectional area (CSA) of cardiomyocytes and decreased the relative vascularity (number of vessels/number of cardiomyocytes/CSA) (Figure 3, A–C), which in turn led to exacerbation of myocardial hypoxia (Figure 3D) and cardiomyocyte death (Figure 3E). In contrast, the increase of CSA after TAC was significantly attenuated by STZ treatment and the relative vascular density was markedly increased (Figure 3, A–C). Consequently, depletion of plasma insulin prevented cardiac hypoxia and cardiomyocyte death during chronic pressure overload (Figure 3, D and E). Conversely, insulin treatment of STZ-treated mice increased CSA and decreased relative vascular density, thereby exacerbating cardiac hypoxia and cardiomyocyte death (Figure 3, A–E). Additional treatment with the proangiogenic factor cartilage oligomeric matrix protein–angiopoietin-1 (COMP-Ang1) (17) increased relative vascular density and thereby improved cardiac hypoxia and systolic dysfunction (Supplemental Figure 5, A–C). We also found that a decrease of relative vascular density was associated with cardiac dysfunction, along with upregulation of insulin signaling in spontaneously hypertensive rats (Supplemental Figure 3, A–G), suggesting that cardiac insulin signaling plays a pathological role in HF by increasing a mismatch between cardiomyocyte size and vascularity.

Cardiomyocyte-specific reduction of Insr expression attenuates systolic dysfunction due to pressure overload. To further investigate the role of cardiac insulin signaling, we generated CIRKO mice by using the Cre-loxP system. We prepared transgenic mice in which a transgene encoding Cre recombinase was driven by the cardiomyocyte-specific α–myosin heavy chain (MHC) promoter (18). We then crossed these MHC-Cre mice with mice bearing floxed *Insr* alleles (19) and produced TAC in the resulting mice. Since homozygous CIRKO ($Insr^{flox/flox}$Cre$^+$) mice have been shown to develop systolic dysfunction in response to pressure overload (6), we utilized heterozygous CIRKO ($Insr^{flox/+}$Cre$^+$) mice with reduced cardiac expression of Insr (Figure 4A). These mice had a normal heart size and normal systolic function under physiological conditions (Figure 4, B and C). However, cardiac insulin signaling was markedly attenuated in the TAC heart of CIRKO mice (Figure 4B), and therefore chronic pressure

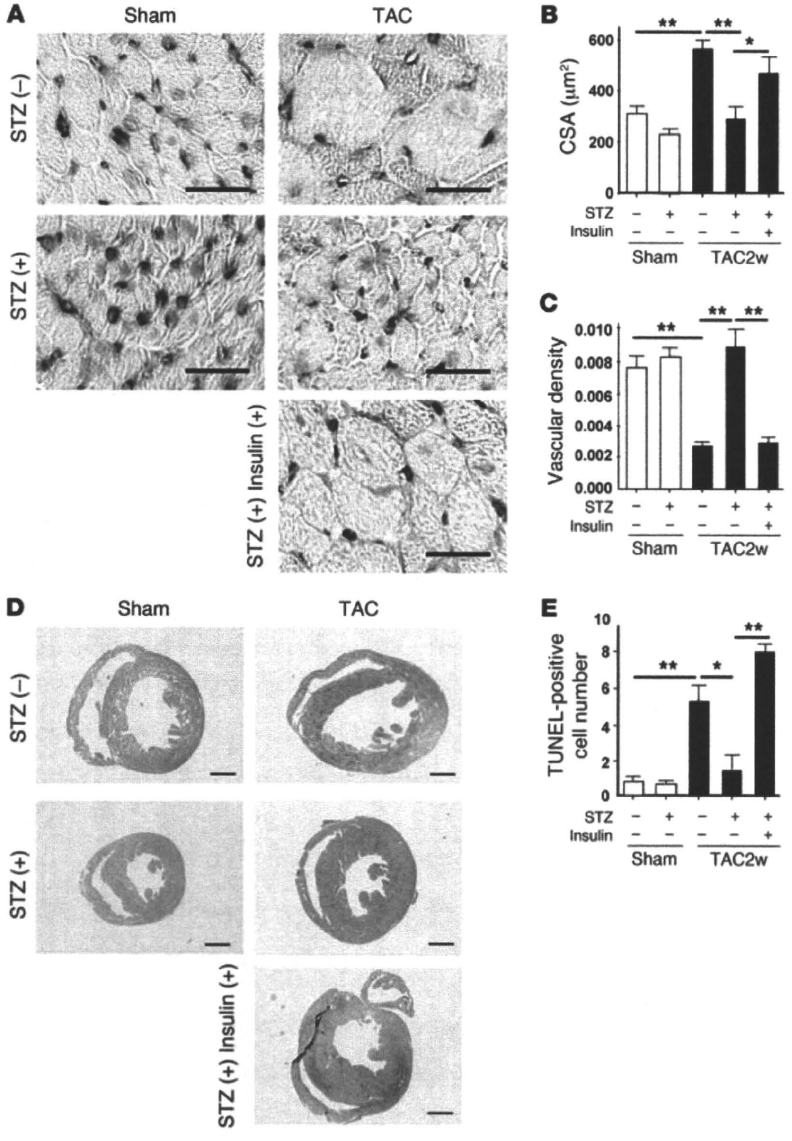

Figure 3

Reduction of plasma insulin inhibits cardiac hypoxia due to pressure overload. (**A**) Animals were prepared as described for Figure 2A. Immunohistochemistry using antibodies against platelet and endothelial cell adhesion molecule (dark brown) and dystrophin (light brown) was performed at 2 weeks after operation. Scale bars: 20 μm. (**B** and **C**) CSA of cardiomyocytes (**B**) and relative vascular density (**C**) were estimated as described in Methods. $n = 4–5$. (**D**) Cardiac ischemia (brown) in mice prepared as described for Figure 2A was estimated with a Hypoxyprobe-1. Scale bars: 1 mm. (**E**) Number of TUNEL-positive cells per 1×10^4 cardiomyocytes. $n = 4–6$. Data are shown as mean ± SEM. $^*P < 0.05$; $^{**}P < 0.01$.

overload caused less severe hypertrophy than in WT mice (Figure 4, C and D). Both systolic dysfunction and left ventricular dilatation were significantly inhibited in CIRKO mice compared with their littermate controls (Figure 4D and Supplemental Figure 6). Histological examination showed that the increase of CSA after TAC was significantly attenuated and relative vascular density was markedly increased in CIRKO mice (Figure 5, A–C). In consequence, the number of dead cardiomyocytes was significantly smaller in CIRKO mice than in their littermate controls (Figure 5D).

To investigate the role of Akt in HF induced by pressure overload, we utilized heterozygous *Akt1*-deficient (*Akt1*$^{+/-}$) mice. Two weeks after TAC operation, both systolic dysfunction and left ventricular dilatation were significantly inhibited in *Akt1*$^{+/-}$ mice compared with their littermate controls (Figure 6A). Histological examination showed that the increase of CSA after TAC was significantly attenuated and relative vascular density was markedly increased in *Akt1*$^{+/-}$ mice (Figure 6, B and C), which was associated with decreased activation of Akt (Figure 6D). These data suggest that sustained activation of Akt could cause cardiac dysfunction under chronic pressure overload.

Mechanism of enhanced cardiac insulin signaling due to pressure overload. To investigate the additional mechanisms by which chronic pressure overload enhances insulin signaling in the heart, we examined pIrs1 levels immediately after TAC. Western blot analysis revealed that pressure overload markedly increased the pIrs1 level from as early as 1 minute after the operation (Figure 7A). Such activation was significantly attenuated in both heterozygous and homozygous CIRKO mice (Figure 7A and Supplemental Figure 7), suggesting that mechanical stress may also upregulate the insulin signaling pathway via direct activation of Insr independent of its ligand. To further investigate the influence of mechanical stress on insulin signaling, we stretched cultured cardiomyocytes by 20% and examined the changes in the pIrs1 level. Consistent with our hypothesis, stretching of cardiomyocytes led to marked activation of insulin sig-

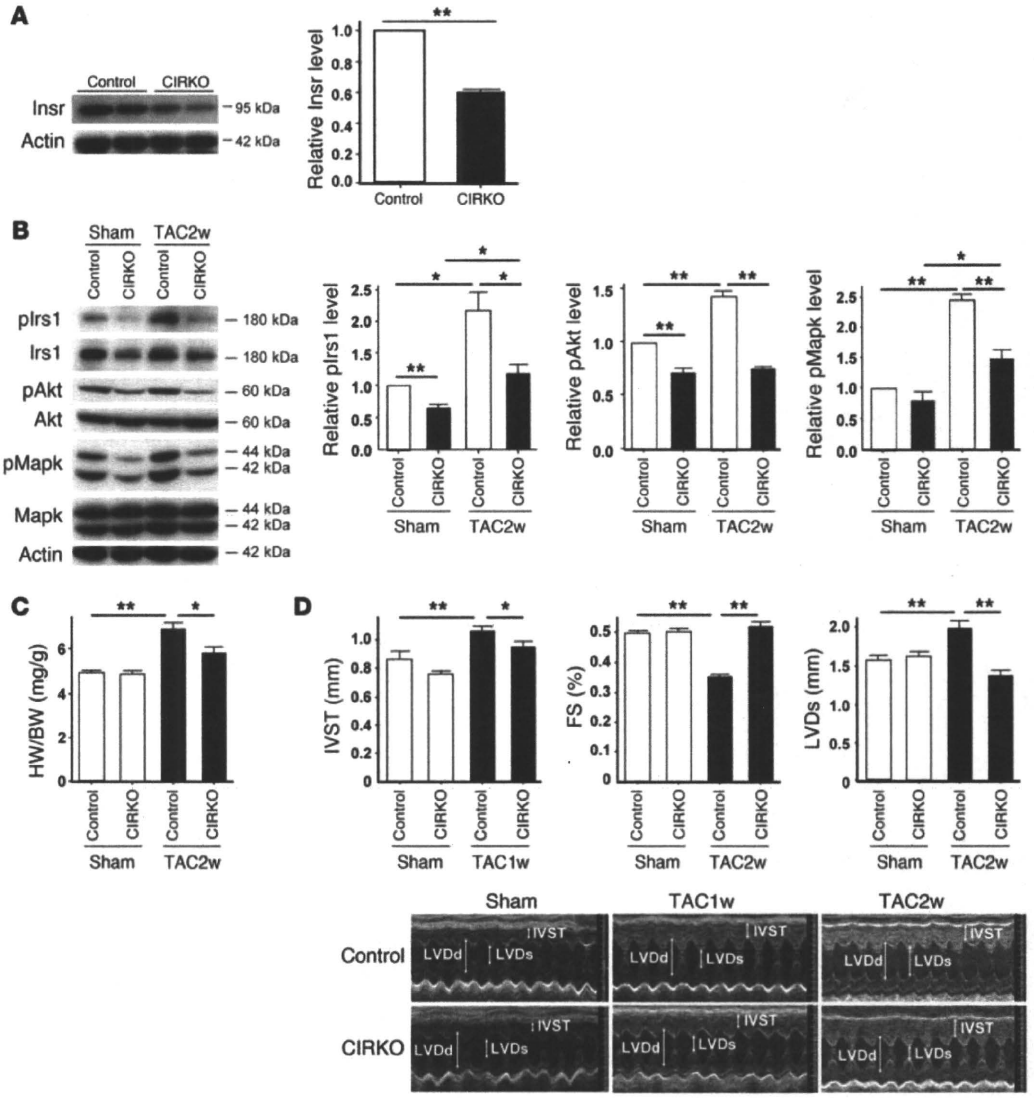

Figure 4

Cardiomyocyte-specific reduction of Insr expression attenuates systolic dysfunction due to pressure overload. (**A**) Western blot analysis of Insr expression in the hearts of CIRKO mice (*Insr*$^{flox/+}$Cre^{+}) and their littermate controls (control). Graphs indicate relative expression levels of Insr. $n = 3$. (**B**) CIRKO mice (*Insr*$^{flox/+}$Cre^{+}) or littermate controls were subjected to TAC or sham operation, and components of the insulin signaling pathway in the heart were examined by Western blot analysis at 2 weeks after operation. Graphs indicate relative expression levels of these signaling molecules. $n = 3$. (**C**) The heart weight/body weight ratio of animals prepared as described in **A** was measured at 2 weeks after operation. $n = 7–9$. (**D**) Cardiac hypertrophy and systolic function of animals prepared as described in **A** were assessed by echocardiography at 1 week (IVST) or 2 weeks (FS and LVDs) after operation. Photographs show representative results of echocardiography (M-mode). $n = 8–13$. Data are shown as mean ± SEM. $^{*}P < 0.05$; $^{**}P < 0.01$.

naling (Figure 7B). This activation was abolished by knockdown of Insr expression (Figure 7C), whereas knockdown of Igf1 or the Igf1 receptor showed a marginal effect (Supplemental Figure 8). These results suggest that mechanical stress mainly enhances insulin signaling through Insr and that Igf1 and the Igf1 receptor contribute to stretch-induced activation of this signaling to a lesser extent. This is similar to the known direct activation of the angiotensin II type I receptor by mechanical stress, which contributes to pathological hypertrophy (20); however, the precise mechanism of how mechanical stress activates insulin signaling needs further investigation.

There is accumulating evidence that suggests a potential relationship between insulin resistance and cardiac hypertrophy (21, 22). Therefore we examined plasma glucose and insulin levels in mice subjected to chronic pressure overload. Both glucose and insulin levels were significantly higher in the TAC group than in the sham-operated group (Figure 7D). More importantly, the homeostasis model assessment–insulin resistance (HOMA-IR) index was markedly elevated in the TAC group (Figure 7D). Furthermore, insulin-induced phosphorylation of Akt was impaired in the liver of the TAC group compared with the sham-operated group (Figure 7E).

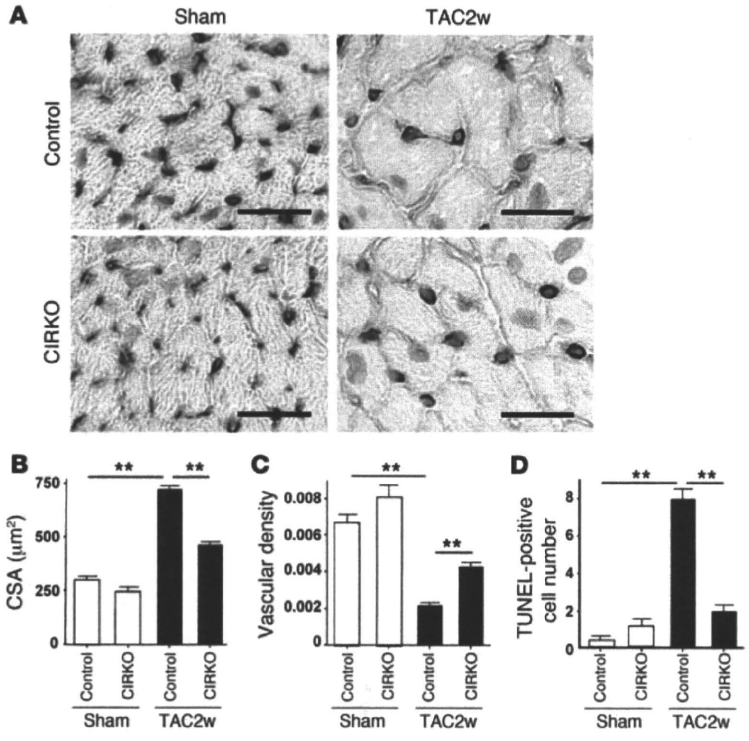

Figure 5
Cardiomyocyte-specific reduction of Insr expression attenuates cardiac hypoxia due to pressure overload. (**A**) CIRKO mice (*Insr*$^{flox/+}$Cre^{+}) or littermate controls were subjected to TAC or sham operation. Immunohistochemistry using antibodies against platelet and endothelial cell adhesion molecules (dark brown) and dystrophin (light brown) was performed at 2 weeks after operation. Scale bars: 20 μm. (**B** and **C**) CSA of cardiomyocytes (**B**) and relative vascular density (**C**) were estimated as described in Methods. $n = 4–5$. (**D**) Number of TUNEL-positive cells per 1×10^4 cardiomyocytes. $n = 4–5$. Data are shown as mean ± SEM. $^*P < 0.05$; $^{**}P < 0.01$.

These results suggest that chronic pressure overload induces hepatic insulin resistance, thereby inducing hyperinsulinemia, whereas there is no cardiac insulin resistance due to direct activation of Insr as well as to upregulation of Insr and Irs1.

Discussion

A number of clinical studies have strongly indicated the link between insulin resistance and nonischemic HF (23–26). Approximately two-thirds of patients with essential hypertension have abnormal glucose metabolism (27), and there is a positive relationship between cardiac hypertrophy and the plasma insulin concentration (28), suggesting that elevation of insulin contributes to myocardial growth in the presence of chronic pressure overload. Consistent with these reports, we found that chronic pressure overload induced hepatic insulin resistance and increased the plasma insulin level. Myocardial stretch activated Insr, and chronic pressure overload not only increased the activity of insulin signaling (pIrs1 and pAkt levels), but also upregulated the expression of Insr and Irs1 protein. This in turn facilitated activation of cardiac insulin signals by hyperinsulinemia. Such activation enhanced the mismatch between vascularity and cardiomyocyte size and increased cardiomyocyte death. This increase was associated with systolic dysfunction and may be one of the causes of HF induced by chronic pressure overload. However, we have not excluded other mechanisms by which excessive insulin signals promote cardiac dysfunction during pressure overload. For example, cardiac hypoxia may affect metabolism and contraction of myocytes with their viability being unchanged. Indeed, we only showed evidence for tissue hypoxia in the TAC heart by using pimonidazole, which may not be sufficient. We have not demonstrated that inhibition of cardiomyocyte death attenuates systolic dysfunction of the TAC heart. Accordingly, we cannot definitively conclude that hypoxia-induced cardiomyocyte death was essential for the development of HF. It has been reported that endothelial cells in the heart release a variety of factors, such as neuregulin and nitric oxide, that regulate survival and function of cardiomyocytes and that endothelial-myocardial interaction plays a crucial role in maintaining systolic function (29). Thus, it is also possible that a decrease of relative vascular density in the TAC heart impairs such paracrine mechanisms, leading to systolic dysfunction.

Our results were similar to those of the study with conditional Akt transgenic animals (14). In this model, Akt signaling could be switched on or off in the heart. These mice developed physiological hypertrophy following short-term induction, but exhibited pathological hypertrophy with longer periods of Akt activation due to an imbalance between cardiac growth and angiogenesis. Interestingly, cardiac dysfunction was further impaired when Akt was switched off after prolonged activation. These results suggest that Akt signaling itself is beneficial for maintenance of systolic function in this model; however, excessive cardiac growth with insufficient angiogenesis causes pathological hypertrophy. Thus, although insulin/Akt signaling has been implicated in the development of physiological hypertrophy, constitutive activation of these signals can induce HF when coordinated tissue growth and angiogenesis are disrupted.

Alterations of myocardial substrate metabolism have been implicated in the pathogenesis of contractile dysfunction and HF (21, 30). Studies on animal models of HF have demonstrated that, during transition from cardiac hypertrophy to ventricular dysfunction, expression of genes encoding for mitochondrial fatty acid (FA) β-oxidation enzymes shows a coordinated decrease, resulting in a shift of myocardial metabolism that recapitulates the fetal heart gene program, with glucose instead of FA becoming the primary energy substrate (31, 32). Clinical studies have revealed that patients with nonischemic cardiomyopathy exhibit alterations of

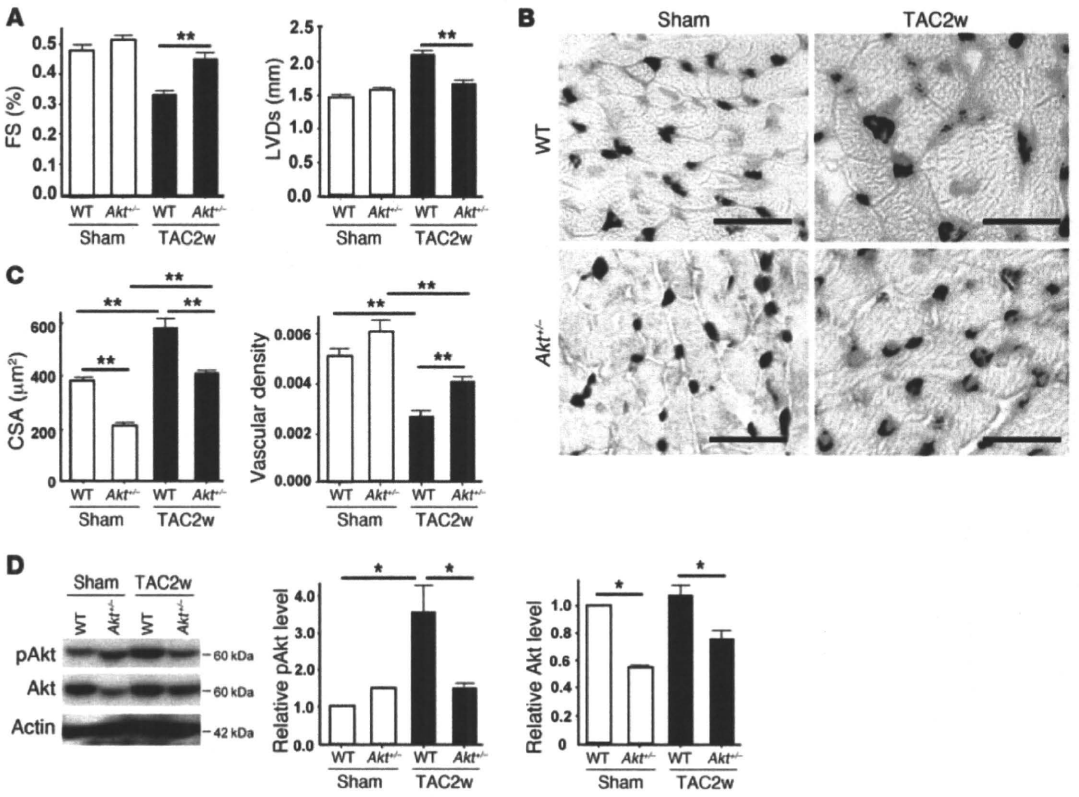

Figure 6

Reduced activation of Akt attenuates systolic dysfunction due to pressure overload. (**A**) *Akt1*-deficient (*Akt1*$^{+/-}$) mice and WT littermates were subjected to TAC or sham operation. Cardiac hypertrophy and systolic function were assessed by echocardiography at 2 weeks after operation. $n = 4–6$. (**B**) Immunohistochemistry using antibodies against platelet and endothelial cell adhesion molecules (dark brown) and dystrophin (light brown) was performed at 2 weeks after operation. Scale bars: 20 μm. (**C**) CSA of cardiomyocytes and relative vascular density were estimated as described in Methods. $n = 3$. (**D**) pAkt and Akt levels in the heart at 2 weeks after operation were examined by Western blot analysis. Graphs indicate relative expression levels of pAkt and Akt. $n = 3$. Data are shown as mean ± SEM. *$P < 0.05$; **$P < 0.01$.

myocardial metabolism that are characterized by a decrease of FA metabolism and an increase of myocardial glucose metabolism, a pattern similar to that shown in animal models of HF (33). Under these conditions, increased FA metabolism in the heart is pathogenic and the extent of abnormal FA metabolism predicts both morphologic changes of the heart and a poor clinical outcome (34). In this respect, activation of the insulin/Akt pathway in the failing heart appears to be an adaptive response, but constitutive activation of this pathway also leads to activation of growth signals that results in dysregulated hypertrophy, cardiac hypoxia, and systolic dysfunction. Thus, a metabolic modulator that increases glucose uptake (or decreases FA metabolism) without activation of insulin signaling would be a better strategy for the treatment of HF because these patients have systemic insulin resistance. Our results also suggest that the use of insulin to control hyperglycemia can be harmful, especially in the setting of pressure overload, a finding that is consistent with the outcome of a recent clinical trial (16).

Multiple counterregulatory hormones and cytokines are upregulated in HF and are likely to play a role in insulin resistance and altered glucose disposition (21). Upregulation of catecholamines not only contributes directly to the pathogenesis of cardiomyopathy but also increases insulin resistance and thereby indirectly affects systolic function. We also found that chronic pressure overload increased the production of proinflammatory cytokines by adipose tissue, thus promoting systemic insulin resistance (I. Shimizu and T. Minamino, unpublished observations). Further investigation of the link between insulin resistance and HF will continue to provide novel insights into the treatment of HF.

Methods

Animal models. All animal study protocols were approved by the Chiba University Review Board. C57BL/6 mice were purchased from SLC Japan. TAC was performed as described previously (15) in 11-week-old male mice. Sham-operated mice underwent the same procedure except for aortic constriction. For the type 1 diabetic model, 7-week-old male C57BL/6 mice were treated with i.p. STZ in 0.1 M sodium citrate (pH 4.5) at a dose of 50 mg/kg for 5 days. TAC was performed 4 weeks after STZ treatment. In the insulin-treated group, mice received daily i.p. injection of insulin (0.1 IU/g/d) from 9 weeks (2 weeks after STZ treatment) to 13 weeks of age (2 weeks after TAC). In some experiments, mice received an i.p. injection of insulin (1 IU/kg) 30 minutes before sacrifice to investigate the insulin sensitivity of various organs. *Akt1*-deficient mice (*Akt1*$^{+/-}$) were a gift from Morris J. Birnbaum (University of Pennsylvania School of Medicine, Philadelphia, Pennsylvania, USA). The generation and genotyping of *Akt1*-deficient mice, floxed *Insr* mice, and MHC-Cre mice have been described previously (18, 19, 35). Littermate controls have the genotype *Insr*$^{flox/+}$ or *Insr*$^{flox/flox}$. We

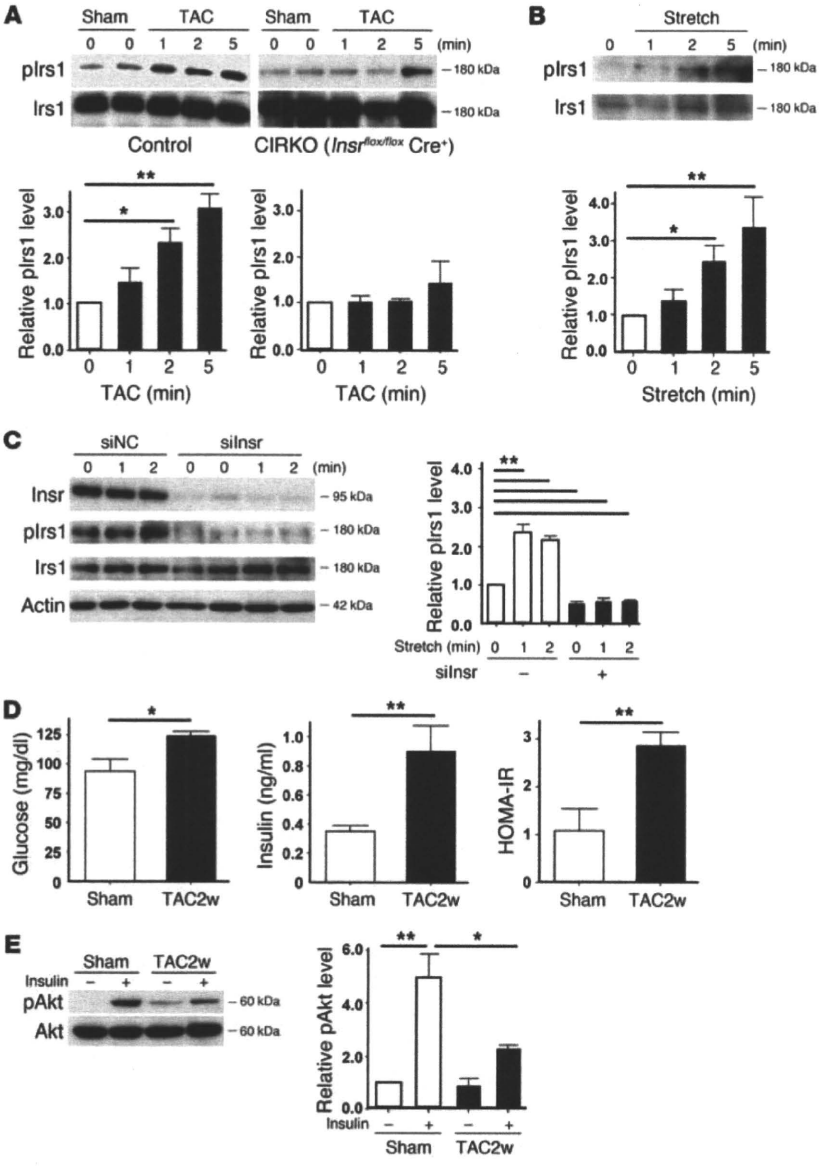

Figure 7

Mechanism of enhanced insulin signaling in the heart during pressure overload. (**A**) CIRKO mice (*Insr*$^{flox/flox}$Cre^{+}) or littermate controls were subjected to TAC or sham operation, and heart samples were obtained at the indicated times. pIrs1 levels were examined by Western blot analysis. The graphs indicate relative expression levels of pIrs1. $n = 3$. (**B**) Cardiomyocytes were subjected to mechanical stretch and pIrs1 levels were examined by Western blot analysis. $n = 3$. (**C**) siRNA targeting Insr (siInsr) or negative control RNA (siNC) was introduced into cardiomyocytes, after which the cells were subjected to mechanical stretch. pIrs1 levels were examined by Western blot analysis. $n = 3$. (**D**) Plasma glucose and insulin levels were examined at 2 weeks after TAC. $n = 7$–8. (**E**) Insulin-induced phosphorylation of Akt (pAkt) in the liver was examined after TAC or sham operation. $n = 3$. Data are shown as mean ± SEM. $^{*}P < 0.05$; $^{**}P < 0.01$.

administered adenoviral vector encoding COMP-Ang1 to mice i.v. after TAC operation as previously described (17).

Physiological and histological analyses. Echocardiography was performed with a Vevo 770 High Resolution Imaging System (Visual Sonics Inc.). To minimize variation of the data, the heart rate was always approximately 500–600 beats per minute when cardiac function was assessed. Cardiac tissue was fixed by perfusion with 4% paraformaldehyde. The fixed sample was immersed in OCT compounds (Miles Inc.) and snap-frozen in liquid nitrogen to prepare cryostat sections. Frozen cross sections of hearts were immunohistochemically double stained with antibodies for PECAM (BD Biosciences — Pharmingen) and dystrophin (Novocastra Laboratories). For measurement of the CSA of cardiomyocytes, 50 randomly selected cardiomyocytes in a left ventricular cross section were measured by tracing dystrophin immunostaining with NIH ImageJ software (http://rsbweb.nih.gov/ij/). Using the same sections, the number of PECAM-positive vessels was counted, and vascular density was estimated as the number of microvessels/number of cardiomyocytes/CSA. Tissue hypoxia was estimated with the Hypoxyprobe-1 (Chemicon) according to the manufacturer's instructions. Briefly, an i.p. injection of pimonidazole (60 mg/kg) was performed 90 minutes before sacrifice. Heart samples were harvested and fixed in 10% formalin overnight. The samples were embedded in paraffin, sectioned at 4-μm thickness, and stained with the Hypoxyprobe-1 monoclonal antibody (clone 4.3.11.3), which binds to protein adducts of pimonidazole in hypoxic cells. TUNEL labeling was performed according to the manufacturer's protocol (In Situ Apoptosis Detection Kit; TaKaRa) in combination with immunostaining for appropriate cell markers.

Western blot analysis. Whole-cell lysates were prepared in lysis buffer (10 mM Tris-HCl, pH 8, 140 mM NaCl, 5 mM EDTA, 0.025% NaN3, 1% Triton X-100, 1% deoxycholate, 0.1% SDS, 1 mM PMSF, 5 μg/ml leupeptin, 2 μg/ml aprotinin, 50 mM NaF, and 1 mM Na_2VO_3). The lysates (40–50 μg) were resolved by SDS-PAGE. Proteins were transferred to a PVDF membrane (Millipore), which was incubated with the primary antibody followed by anti-rabbit or anti-mouse immunoglobulin-G conjugated with horseradish peroxidase (Jackson). Specific proteins were detected by enhanced chemiluminescence

(Amersham). The primary antibodies used for Western blotting were as follows: anti-pIrs1 antibody (Tyr612, Biomol), anti-Irs1 antibody (C20), anti-Akt1 antibody (C20), anti-Insr β antibody (C-19) (Santa Cruz Biotechnology Inc.), anti-phospho-Akt antibody (Ser473), anti-phospho-p44/42 MAP kinase antibody (Thr202/Tyr204), anti-MAP kinase (ERK1+ERK2) antibody (Invitrogen), and anti-actin antibody (Sigma-Aldrich). Plasma insulin levels were evaluated with an ELISA kit (Morinaga Institute of Biological Science Inc.) according to the manufacturer's instructions.

Cell culture. Neonatal Wistar rats were purchased from Takasugi Experimental Animal Supply. Cardiomyocytes were prepared from neonatal rats and cultured as described previously (15). Passive stretching of cultured cells was done as described previously. Cells were plated on collagen-coated silicone rubber dishes (STREX Mechanical Cell Strain Instruments), and the silicone dishes were stretched by attaching both ends of each dish firmly to a fixed frame, resulting in longitudinal stretch by 20% of the original length. siRNA targeting Insr, IGF, and the IGF-1 receptor was purchased from Invitrogen and introduced into rat cardiomyocytes by using Lipofectamine RNAiMax (Invitrogen) according to the manufacturer's instructions.

Statistics. Data are shown as the mean ± SEM. Differences between groups were examined by 2-tailed Student's *t* test or ANOVA, followed by Bonferroni's correction for comparison of means. For all analyses, $P < 0.05$ was considered statistically significant.

Acknowledgments

We thank Morris J. Birnbaum for *Akt1*-deficient mice. This work was supported by a Grant-in-Aid for Scientific Research from the Ministry of Education, Science, Sports, and Culture and Health and Labor Sciences research grants (to I. Komuro); a Grant-in-Aid for Scientific Research from the Ministry of Education, Culture, Sports, Science and Technology of Japan; and grants from the Suzuken Memorial Foundation; the Japan Diabetes Foundation; the Ichiro Kanehara Foundation; the Tokyo Biochemical Research Foundation; the Takeda Science Foundation; the Cell Science Research Foundation; the Japan Foundation of Applied Enzymology; and the Astellas Foundation for Research on Metabolic Disorders (to T. Minamino).

Received for publication June 5, 2009, and accepted in revised form February 10, 2010.

Address correspondence to: Issei Komuro, Department of Cardiovascular Science and Medicine, Chiba University Graduate School of Medicine, 1-8-1 Inohana, Chuo-ku, Chiba 260-8670, Japan. Phone: 81.43.226.2097; Fax: 81.43.226.2557; E-mail: komuro-tky@umin.ac.jp.

1. Frey N, Olson EN. Cardiac hypertrophy: the good, the bad, and the ugly. *Annu Rev Physiol.* 2003;65:45–79.
2. Adams TD, Yanowitz FG, Fisher AG, Ridges JD, Lovell K, Pryor TA. Noninvasive evaluation of exercise training in college-age men. *Circulation.* 1981; 64(5):958–965.
3. Pelliccia A, Maron BJ. Outer limits of the athlete's heart, the effect of gender, and relevance to the differential diagnosis with primary cardiac diseases. *Cardiol Clin.* 1997;15(3):381–396.
4. Heineke J, Molkentin JD. Regulation of cardiac hypertrophy by intracellular signalling pathways. *Nat Rev Mol Cell Biol.* 2006;7(8):589–600.
5. Belke DD, et al. Insulin signaling coordinately regulates cardiac size, metabolism, and contractile protein isoform expression. *J Clin Invest.* 2002; 109(5):629–639.
6. Hu P, Zhang D, Swenson L, Chakrabarti G, Abel ED, Litwin SE. Minimally invasive aortic banding in mice: effects of altered cardiomyocyte insulin signaling during pressure overload. *Am J Physiol Heart Circ Physiol.* 2003;285(3):H1261–H1269.
7. Shioi T, et al. The conserved phosphoinositide 3-kinase pathway determines heart size in mice. *EMBO J.* 2000;19(11):2537–2548.
8. McMullen JR, et al. Phosphoinositide 3-kinase (p110α) plays a critical role for the induction of physiological, but not pathological, cardiac hypertrophy. *Proc Natl Acad Sci U S A.* 2003;100(21):12355–12360.
9. DeBosch B, et al. Akt1 is required for physiological cardiac growth. *Circulation.* 2006;113(17):2097–2104.
10. Samuelsson AM, et al. Hyperinsulinemia: effect on cardiac mass/function, angiotensin II receptor expression, and insulin signaling pathways. *Am J Physiol Heart Circ Physiol.* 2006;291(2):H787–H796.
11. Condorelli G, et al. Akt induces enhanced myocardial contractility and cell size in vivo in transgenic mice. *Proc Natl Acad Sci U S A.* 2002;99(19):12333–12338.
12. Matsui T, et al. Phenotypic spectrum caused by transgenic overexpression of activated Akt in the heart. *J Biol Chem.* 2002;277(25):22896–22901.
13. Shioi T, et al. Akt/protein kinase B promotes organ growth in transgenic mice. *Mol Cell Biol.* 2002; 22(8):2799–2809.
14. Shiojima I, et al. Disruption of coordinated cardiac hypertrophy and angiogenesis contributes to the transition to heart failure. *J Clin Invest.* 2005; 115(8):2108–2118.
15. Sano M, et al. p53-induced inhibition of Hif-1 causes cardiac dysfunction during pressure overload. *Nature.* 2007;446(7134):444–448.
16. Gerstein HC, et al. Effects of intensive glucose lowering in type 2 diabetes. *N Engl J Med.* 2008; 358(24):2545–2559.
17. Cho CH, et al. Long-term and sustained COMP-Ang1 induces long-lasting vascular enlargement and enhanced blood flow. *Circ Res.* 2005;97(1):86–94.
18. Abel ED, et al. Cardiac hypertrophy with preserved contractile function after selective deletion of GLUT4 from the heart. *J Clin Invest.* 1999;104(12):1703–1714.
19. Bruning JC, et al. A muscle-specific insulin receptor knockout exhibits features of the metabolic syndrome of NIDDM without altering glucose tolerance. *Mol Cell.* 1998;2(5):559–569.
20. Zou Y, et al. Mechanical stress activates angiotensin II type 1 receptor without the involvement of angiotensin II. *Nat Cell Biol.* 2004;6(6):499–506.
21. Witteles RM, Fowler MB. Insulin-resistant cardiomyopathy clinical evidence, mechanisms, and treatment options. *J Am Coll Cardiol.* 2008;51(2):93–102.
22. Sharma N, Okere IC, Duda MK, Chess DJ, O'Shea KM, Stanley WC. Potential impact of carbohydrate and fat intake on pathological left ventricular hypertrophy. *Cardiovasc Res.* 2007;73(2):257–268.
23. Swan JW, et al. Insulin resistance in chronic heart failure: relation to severity and etiology of heart failure. *J Am Coll Cardiol.* 1997;30(2):527–532.
24. Ingelsson E, Sundstrom J, Arnlov J, Zethelius B, Lind L. Insulin resistance and risk of congestive heart failure. *JAMA.* 2005;294(3):334–341.
25. Arnlov J, et al. Several factors associated with the insulin resistance syndrome are predictors of left ventricular systolic dysfunction in a male population after 20 years of follow-up. *Am Heart J.* 2001; 142(4):720–724.
26. Hasegawa S, Kusuoka H, Maruyama K, Nishimura T, Hori M, Hatazawa J. Myocardial positron emission computed tomographic images obtained with fluorine-18 fluoro-2-deoxyglucose predict the response of idiopathic dilated cardiomyopathy patients to beta-blockers. *J Am Coll Cardiol.* 2004; 43(2):224–233.
27. Garcia-Puig J, Ruilope LM, Luque M, Fernandez J, Ortega R, Dal-Re R. Glucose metabolism in patients with essential hypertension. *Am J Med.* 2006; 119(4):318–326.
28. Karason K, Sjostrom L, Wallentin I, Peltonen M. Impact of blood pressure and insulin on the relationship between body fat and left ventricular structure. *Eur Heart J.* 2003;24(16):1500–1505.
29. Brutsaert DL. Cardiac endothelial-myocardial signaling: its role in cardiac growth, contractile performance, and rhythmicity. *Physiol Rev.* 2003;83(1):59–115.
30. Neubauer S. The failing heart--an engine out of fuel. *N Engl J Med.* 2007;356(11):1140–1151.
31. Christe ME, Rodgers RL. Altered glucose and fatty acid oxidation in hearts of the spontaneously hypertensive rat. *J Mol Cell Cardiol.* 1994;26(10):1371–1375.
32. Barger PM, Kelly DP. Fatty acid utilization in the hypertrophied and failing heart: molecular regulatory mechanisms. *Am J Med Sci.* 1999;318(1):36–42.
33. Davila-Roman VG, et al. Altered myocardial fatty acid and glucose metabolism in idiopathic dilated cardiomyopathy. *J Am Coll Cardiol.* 2002;40(2):271–277.
34. Yazaki Y, et al. Assessment of myocardial fatty acid metabolic abnormalities in patients with idiopathic dilated cardiomyopathy using 123I BMIPP SPECT: correlation with clinicopathological findings and clinical course. *Heart.* 1999;81(2):153–159.
35. Cho H, Thorvaldsen JL, Chu Q, Feng F, Birnbaum MJ. Akt1/PKBalpha is required for normal growth but dispensable for maintenance of glucose homeostasis in mice. *J Biol Chem.* 2001;276(42):38349–38352.

Research article

Sonic hedgehog is a critical mediator of erythropoietin-induced cardiac protection in mice

Kazutaka Ueda,[1] Hiroyuki Takano,[1] Yuriko Niitsuma,[1,2] Hiroshi Hasegawa,[1] Raita Uchiyama,[1] Toru Oka,[1] Masaru Miyazaki,[2] Haruaki Nakaya,[3] and Issei Komuro[1]

[1]Department of Cardiovascular Science and Medicine, [2]Department of General Surgery, and [3]Department of Pharmacology, Chiba University Graduate School of Medicine, Chiba, Japan.

Erythropoietin reportedly has beneficial effects on the heart after myocardial infarction, but the underlying mechanisms of these effects are unknown. We here demonstrate that sonic hedgehog is a critical mediator of erythropoietin-induced cardioprotection in mice. Treatment of mice with erythropoietin inhibited left ventricular remodeling and improved cardiac function after myocardial infarction, independent of erythropoiesis and the mobilization of bone marrow–derived cells. Erythropoietin prevented cardiomyocyte apoptosis and increased the number of capillaries and mature vessels in infarcted hearts by upregulating the expression of angiogenic cytokines such as VEGF and angiopoietin-1 in cardiomyocytes. Erythropoietin also increased the expression of sonic hedgehog in cardiomyocytes, and inhibition of sonic hedgehog signaling suppressed the erythropoietin-induced increase in angiogenic cytokine expression. Furthermore, the beneficial effects of erythropoietin on infarcted hearts were abolished by cardiomyocyte-specific deletion of sonic hedgehog. These results suggest that erythropoietin protects the heart after myocardial infarction by inducing angiogenesis through sonic hedgehog signaling.

Introduction

Recent medical advances have improved survival rates of patients with acute myocardial infarction (MI), whereas the number of patients showing heart failure after MI has increased in recent years (1). LV remodeling, which includes dilatation of the ventricle and increased interstitial fibrosis, is the critical process that underlies the progression to heart failure (1). Although pharmacological therapies are effective, heart failure is still one of the leading causes of death worldwide (2). It is thus important to elucidate a novel approach to prevent LV remodeling after MI.

Several hematopoietic cytokines including erythropoietin (EPO), G-CSF, and stem cell factor have been reported to prevent cardiac remodeling and dysfunction after MI in various animal models (3–5). EPO, a major regulator of erythroid progenitors, has attracted great attention because its administration induced significant improvements in the clinical status and LV function of patients with congestive heart failure (6, 7). Although several mechanisms of cardioprotective effects by EPO have been suggested, the precise mechanisms remain largely unknown (8–14). Treatment with EPO reverses the decreased oxygen-carrying capacity associated with anemia, which is often observed in patients with heart failure (8). EPO has also been reported to mobilize endothelial progenitor cells (EPCs) from bone marrow, leading to neovascularization in the heart (9). In addition, since EPO receptors (EPORs) are expressed in various types of cells including cardiomyocytes, EPO may have direct protective effects on cardiomyocytes (10–14).

In the present study, we investigated the mechanisms of how EPO induced cardioprotection after MI. We observed that EPO directly prevented apoptotic death of cardiomyocytes and enhanced the expression of angiogenic cytokines, which induced robust angiogenesis, leading to the improvement of contractile function after MI. EPO also increased expression levels of sonic hedgehog (Shh) in cardiomyocytes, and the inhibition of Shh signaling abolished the EPO-induced increases of angiogenic cytokine production in cardiomyocytes. In hearts of cardiac-specific inducible Shh knockout (Shh-MerCre) mice, EPO treatment failed to upregulate angiogenic cytokines, enhance angiogenesis, and inhibit LV remodeling. Our results suggest that Shh is a key mediator of EPO-evoked cardioprotection in infarcted hearts.

Results

EPO prevents cardiac remodeling after MI. We subcutaneously administered EPO (10,000 U/kg/d) or saline immediately after coronary artery ligation until 4 days after MI. Fourteen days after MI, we histologically assessed the infarct size and examined cardiac function using echocardiography. Treatment with EPO significantly prevented enlargement of LV end-diastolic dimension (LVEDD) and reduction of fractional shortening (FS) and reduced the infarct size (fibrotic area/LV free wall) compared with saline treatment (Figure 1, A and B), suggesting that EPO prevents LV remodeling and dysfunction after MI.

The role of hematopoietic effects of EPO in cardioprotection (6, 7) was examined using transgene-rescued EPOR-null (RES) mice, which express EPORs only in the hematopoietic lineage (15). Although EPO treatment increased blood hemoglobin levels 7 days after MI in both WT and RES mice (Figure 2A), the cardioprotective effects of EPO were observed only in WT mice but not in the RES mice (Figure 1 and Figure 2B). EPO and saline did not show any significant differences in LVEDD, FS, or infarct size in the RES mice (Figure 2B), suggesting that erythropoiesis is not involved in the cardioprotective effects of EPO.

Authorship note: Kazutaka Ueda, Hiroyuki Takano, and Yuriko Niitsuma contributed equally to this work.

Conflict of interest: The authors have declared that no conflict of interest exists.

Citation for this article: *J Clin Invest.* 2010;120(6):2016–2029. doi:10.1172/JCI39896.

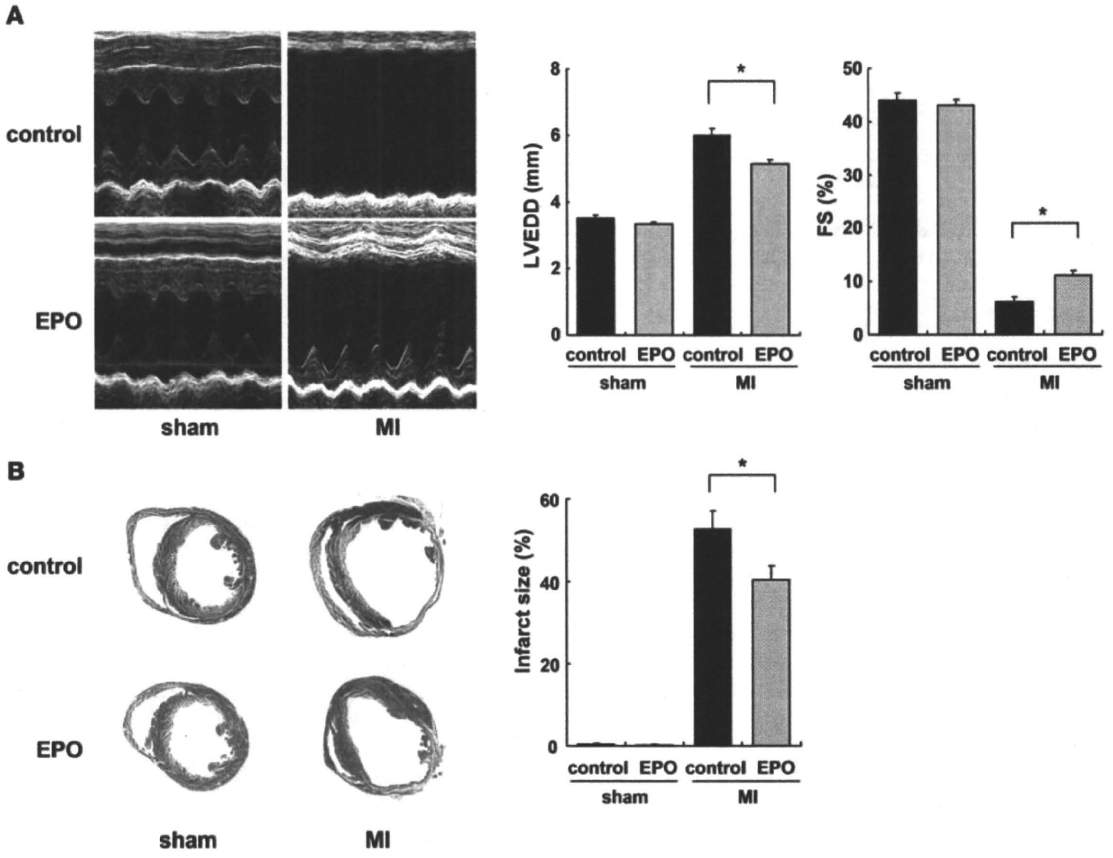

Figure 1
EPO prevents cardiac remodeling after MI. The effects of EPO treatment on LV function and infarct size were examined 14 days after operation. WT mice were subjected to MI or sham operation and treated with EPO or saline (control). (**A**) Echocardiographic analysis. (n = 8–10). (**B**) Masson trichrome staining of hearts and infarct size (n = 8–10). *P < 0.01.

To investigate whether EPO affects responses of inflammation and wound healing that may have an impact on LV remodeling after MI (16, 17), we examined macrophage infiltration and myofibroblast accumulation in the ischemic area after MI by immunohistochemical staining. The number of Mac3-positive macrophages was markedly decreased by EPO treatment 14 days after MI (Supplemental Figure 1A; supplemental material available with this article; doi:10.1172/JCI39896DS1). The number of α-SMA–positive myofibroblasts was significantly increased in EPO-treated hearts compared with saline-treated hearts (Supplemental Figure 1B).

We next determined whether EPO induced the mobilization of EPCs from bone marrow into peripheral blood using flow cytometry (9). After MI, EPO significantly increased the number of circulating CD34/Flk-1–double-positive EPCs in WT mice but not in the RES mice (Figure 2C). We produced MI in WT mice in which the bone marrow was replaced with cells derived from GFP-expressing mice. The hearts were excised 7 and 14 days after MI and immunohistochemically stained for PECAM. There were no differences in the number of GFP-positive cells and GFP/PECAM–double-positive cells in the border areas of EPO- and saline-treated infarcted hearts (Figure 2D), indicating that EPO did not enhance the homing of bone marrow–derived cells or increase the number of bone marrow–derived endothelial cells in the damaged hearts, although EPO induced mobilization of EPCs from bone marrow into peripheral circulation. In addition, EPO did not improve cardiac function or increase the number of vessels in infarcted hearts even in RES mice transplanted with bone marrow of WT mice (Figure 2E). It is thus unlikely that the EPO-mobilized bone marrow–derived cells contribute to the cardioprotective effects of EPO.

EPO inhibits cardiomyocyte apoptosis in infarcted hearts. Apoptotic death of cardiomyocytes has been suggested to cause LV remodeling and dysfunction (18). To determine the role of antiapoptotic effects of EPO in cardioprotection, we performed TUNEL staining of hearts 24 hours after MI. The number of TUNEL-positive cardiomyocytes in the border area was significantly smaller in EPO-treated mice than in saline-treated mice, while EPO treatment had no effect on cardiomyocyte apoptosis in RES mice (Figure 3A). Western blot analysis showed that EPO treatment markedly reduced the level of cleaved caspase-3 in hearts at 24 hours after MI (Figure 3B). TUNEL staining revealed that pretreatment with EPO significantly attenuated H_2O_2-induced apoptotic death in cultured cardiomyocytes of neonatal rats (Figure 3C). At 24 hours after exposing cardiomyocytes to H_2O_2, expression levels of the antiapoptotic protein Bcl-2 were decreased, whereas levels of cleaved caspase-3 were increased, and these changes were inhibited markedly by EPO pretreatment (Figure 3D). Annexin V staining

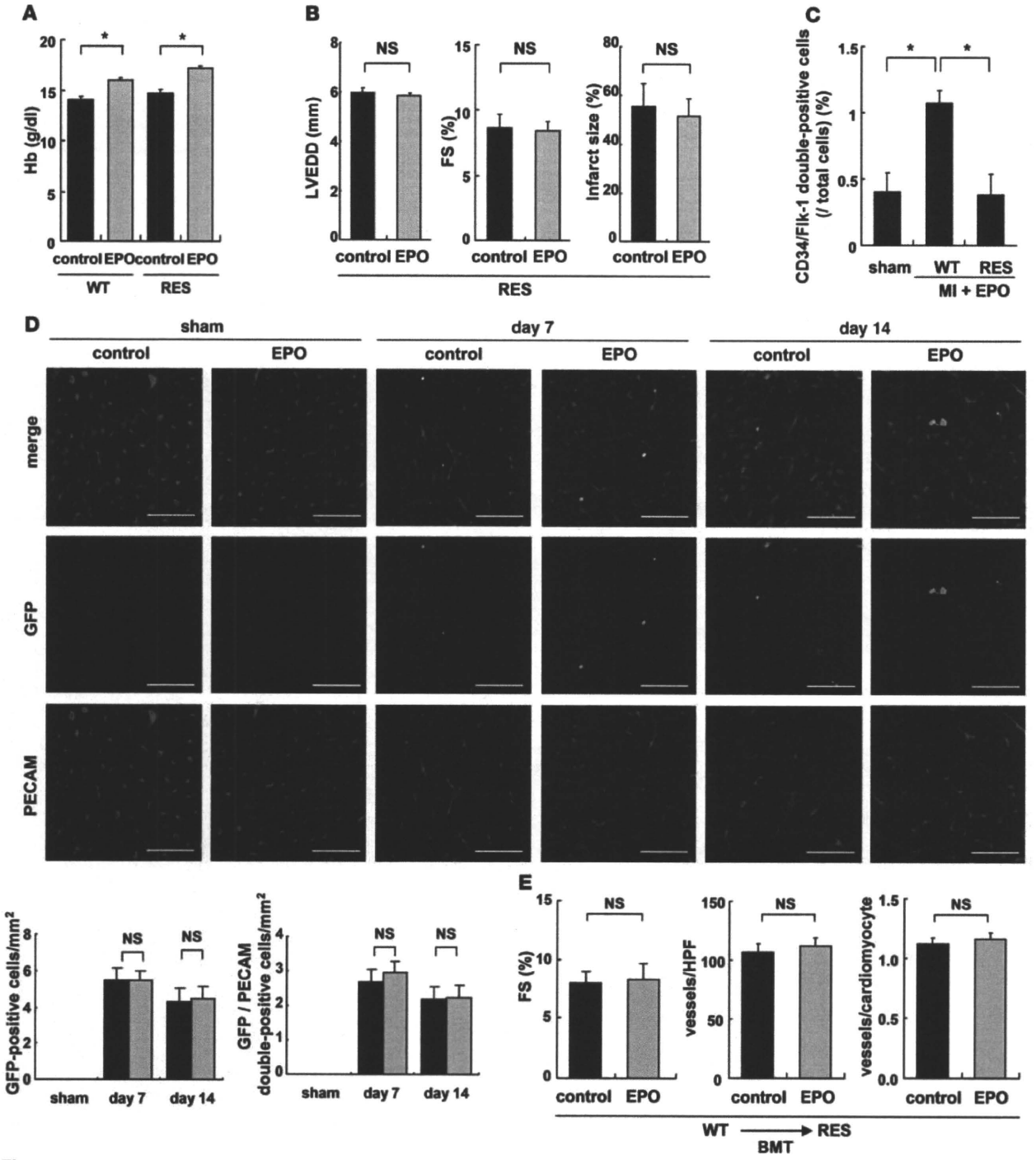

Figure 2

Erythroid hematogenesis is not required for the protective effects of EPO, and EPO does not accelerate the cardiac homing of bone marrow–derived cells after MI. WT and RES mice were subjected to MI and treated with EPO or saline (control). (**A**) Blood hemoglobin (Hb) levels 7 days after MI ($n = 4$). *$P < 0.01$. (**B**) Echocardiography and Masson trichrome staining were performed to analyze LV function and infarct size ($n = 10$). (**C**) Following MI and EPO treatment, the number of circulating CD34/Flk-1–double-positive EPCs increased in WT mice but not in RES mice. *$P < 0.05$ ($n = 4$). (**D**) Bone marrow cells from GFP-expressing mice were transplanted into WT mice. 7 and 14 days after MI, immunohistochemical staining for PECAM (red) was performed, and nuclei were counterstained with TO-PRO-3 (blue). GFP-positive cells (green) represent bone marrow–derived cells that moved into the heart and GFP/PECAM–double-positive cells denote bone marrow–derived endothelial cells. The numbers of GFP– and GFP/PECAM–double-positive cells in the border area (MI group) or LV free wall (sham group) were counted ($n = 5$–8). Scale bars: 50 μm. (**E**) WT bone marrow cells were transplanted (BMT) into RES mice, MI was induced, and the mice were treated with EPO or saline (control). FS, the number of vessels, and the ratio of vessels to cardiomyocytes in the border area are shown ($n = 8$).

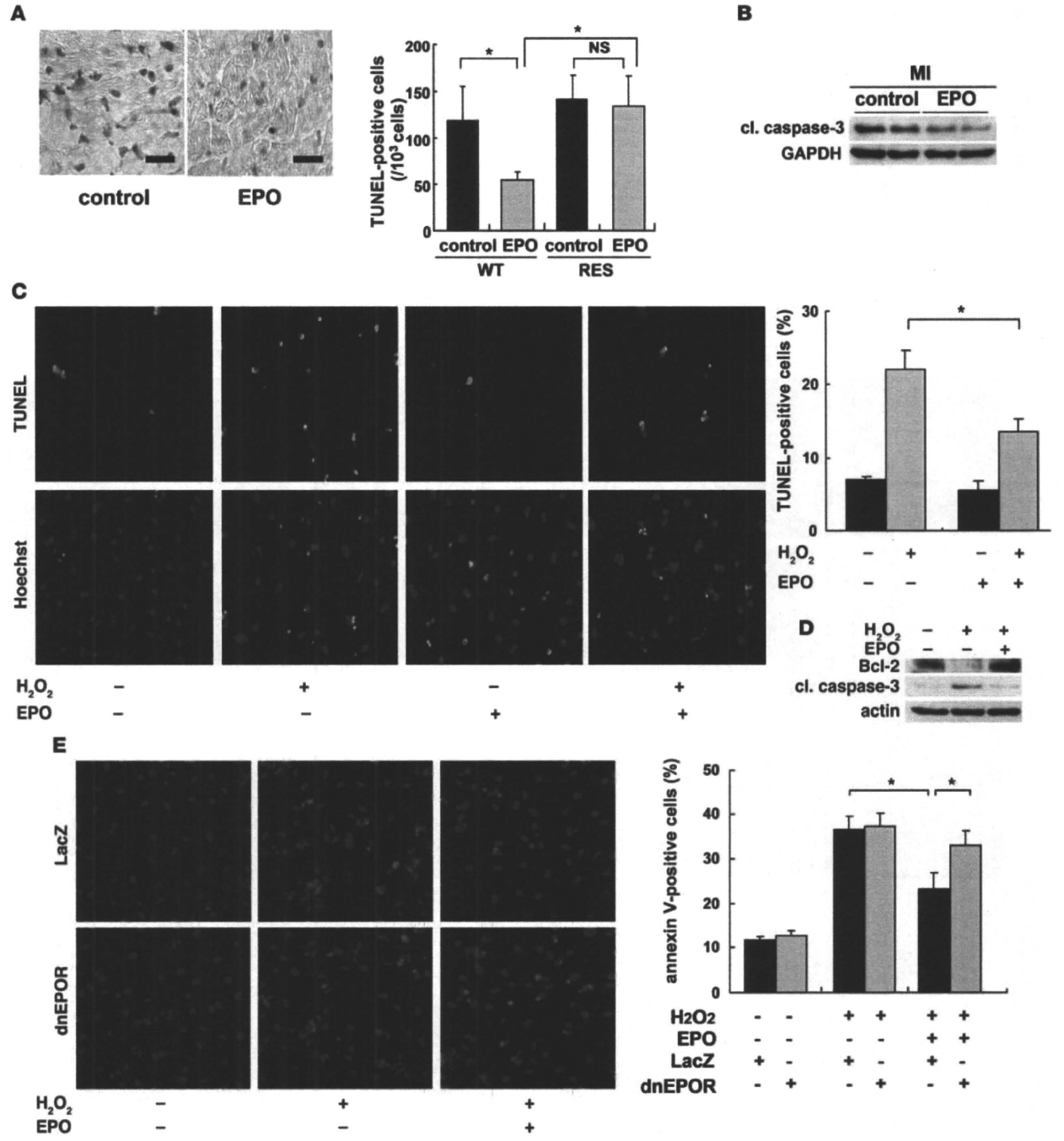

Figure 3

EPO inhibits cardiomyocyte apoptosis in infarcted hearts. (**A**) TUNEL staining (brown) of infarcted hearts from WT mice 24 hours after ligation. Scale bars: 100 μm. The number of TUNEL-positive cardiomyocytes in the border area was counted. *$P < 0.01$ ($n = 10$). (**B**) Representative Western blots of cleaved caspase-3 (cl. caspase-3) protein in the heart 24 hours after MI are shown ($n = 4$). (**C**) Detection of apoptotic cardiomyocytes using FITC-labeled TUNEL staining (green). Nuclei were counterstained with Hoechst 33258 (blue). The TUNEL-positive cardiomyocytes were counted ($n = 10$). *$P < 0.05$. (**D**) Samples were pretreated with EPO for 8 hours before H_2O_2 treatment, and the expression of Bcl-2 and cleaved caspase-3 24 hours after H_2O_2 treatment was analyzed by Western blotting. Representative results from 3 experiments are shown. (**E**) Detection of apoptotic cardiomyocytes using Cy-3–labeled annexin V staining (red). Nuclei were counterstained with Hoechst 33258 (blue). Cardiomyocytes were infected with adenoviral vectors encoding dominant negative form of EPOR or LacZ at 10 MOI. The number of annexin V–positive cardiomyocytes was counted ($n = 10$). *$P < 0.05$.

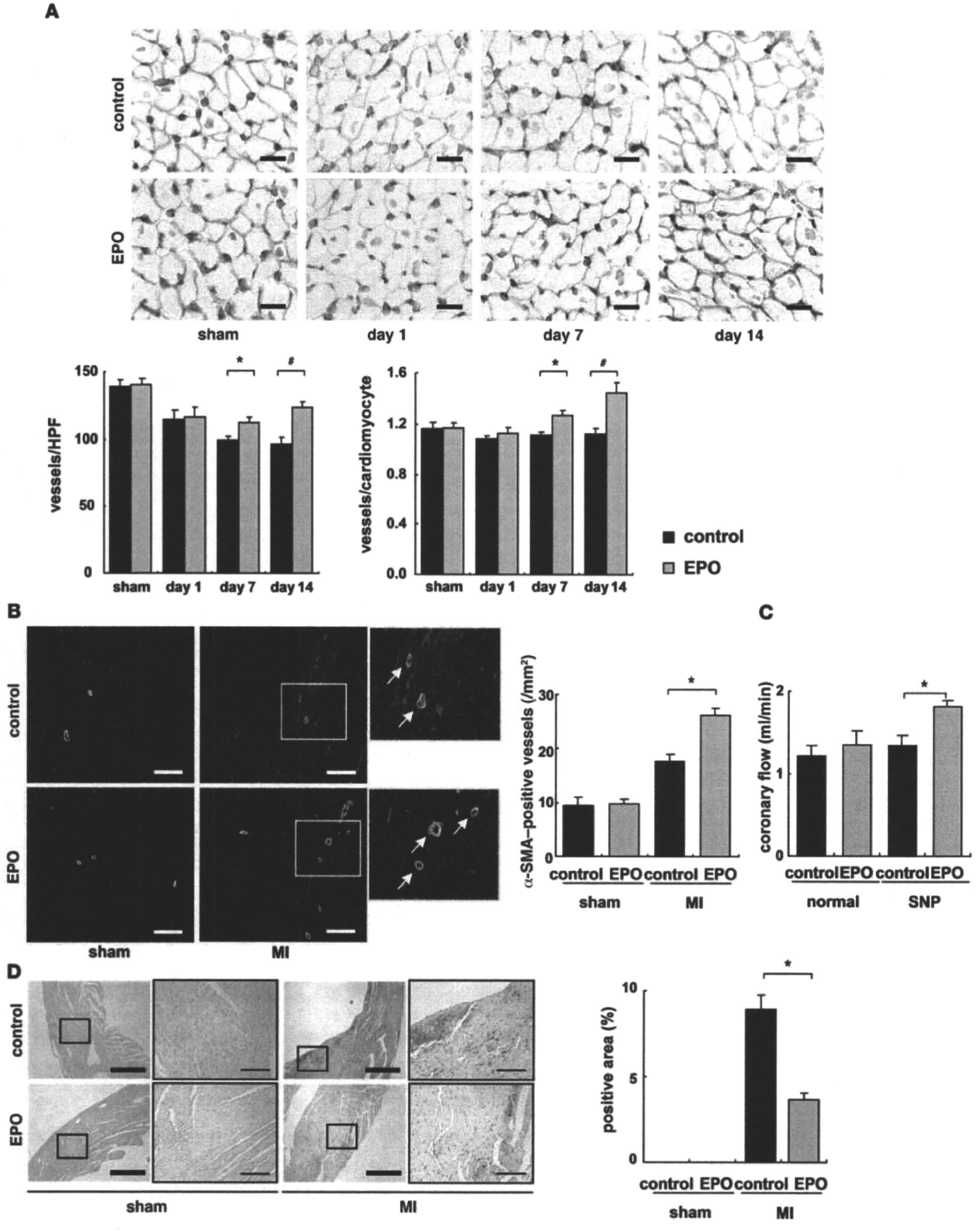
A
control
EPO
sham
day 1
day 7
day 14
vessels/HPF
150
100
50
0
*
#
vessels/cardiomyocyte
1.6
1.2
0.8
0.4
0.0
control
EPO
B
C
α-SMA–positive vessels (/mm²)
30
20
10
0
control EPO control EPO
sham
MI
coronary flow (ml/min)
2
1
0
control EPO control EPO
normal
SNP
D
positive area (%)
10
5
0
control EPO control EPO
sham
MI

Figure 4
EPO promotes angiogenesis in infarcted hearts. (**A**) Double immunostaining for PECAM (green) and dystrophin (brown) in the border area (MI group) or LV free wall (sham group) of EPO- and saline-treated (control) hearts. Scale bars: 20 μm. The number of vessels and the ratio of vessels to cardiomyocyte were measured ($n = 8$ for each). $^*P < 0.05$; $^{\#}P < 0.01$. (**B**) Double immunohistochemical staining for α SMA (green) and PECAM (red) shown together with TO-PRO-3 (blue) staining in the border area (MI group) or LV free wall (sham group) 14 days after operation. The number of α-SMA–positive vessels in the ischemic area was determined ($n = 8$). Scale bars: 100 μm. $^*P < 0.05$. (**C**) Coronary flow was measured in EPO- and saline-treated (control) hearts 14 days after MI with or without sodium nitroprusside (SNP, 10^{-4} M) ($n = 6$). $^*P < 0.05$. (**D**) Representative images of hypoxyprobe staining (brown) of EPO- and saline-treated (control) hearts in the border area (MI group) or LV free wall (sham group) 7 days after operation. The rate of hypoxyprobe-positive area in the border area was measured ($n = 3$). Scale bars: 500 μm (thick bars); 100 μm (thin bars). $^*P < 0.01$.

showed that EPO-induced antiapoptotic effects were abolished by transducing adenoviral vectors, which encode the dominant negative form of EPOR (Figure 3E). These results suggest that EPO accomplishes antiapoptotic effects on cardiomyocytes through the EPO/EPOR signaling pathways. EPO has been reported to activate several kinases including Akt and ERK, which promote cell surviving pathways (10, 19). We thus determined whether EPO inhibits the death of cardiomyocytes by activating these kinases. Indeed, both Akt and ERK were activated in cultured cardiomyocytes by EPO in a time- and dose-dependent manner, and these activations were abolished by transducing dominant negative EPOR (Supplemental Figure 2, A–C). Inhibitions of Akt and ERK using respective kinase inhibitors suppressed EPO-induced reduction in the number of TUNEL-positive cardiomyocytes and EPO-induced downregulation of cleaved caspase-3 (Supplemental Figure 2, D and E), suggesting that EPO prevents apoptotic death of cardiomyocytes at least in part by activating Akt and ERK through the EPO/EPOR system in cardiomyocytes.

Angiogenic cytokines mediate EPO-induced cardioprotection. To determine the angiogenic effects of EPO, we performed immunohistochemical double-staining of infarcted hearts for PECAM and dystrophin. EPO treatment markedly increased the number of PECAM-positive capillary vessels and the ratio of vessels to cardiomyocytes in the border area at 7 days after MI (Figure 4A). Moreover, EPO significantly increased the number of α-SMA–positive vessels in the heart 14 days after MI (Figure 4B), suggesting that EPO induces the formation of mature vessels in infarcted hearts.

We also investigated the effects of EPO-induced angiogenesis on myocardial perfusion. At 14 days after MI, the coronary flow under dilatory stimulation with sodium nitroprusside was significantly increased in EPO-treated hearts compared with saline-treated hearts in the isolated heart perfusion system (Figure 4C). The extent of myocardial ischemia in the border area detected by Hypoxyprobe staining was decreased by EPO treatment (Figure 4D), suggesting that EPO-induced angiogenesis is functionally relevant to the enhancement of coronary perfusion reserve and the reduction of cardiac ischemia in infarcted hearts. Meanwhile, there were no significant differences in the cross-sectional area of cardiomyocytes in the border area at 14 days after MI between EPO and saline treatment (Supplemental Figure 3).

We also examined the mechanisms of EPO-induced angiogenesis in vitro using HUVECs. The administration of EPO did not increase BrdU incorporation into HUVECs. In contrast, the culture medium of cardiomyocytes conditioned by EPO markedly enhanced the BrdU incorporation into HUVECs compared with the cultured medium of cardiomyocytes conditioned by saline (Figure 5A). The conditioned medium from EPO-treated cardiomyocytes also significantly enhanced tube formation of HUVECs, whereas the administration of EPO itself did not affect tube formation of HUVECs cultured in the medium from saline-treated cardiomyocytes (Figure 5B). These results suggest that EPO evokes an angiogenic response by inducing paracrine factors secreted from cardiomyocytes.

EPO upregulated the levels of VEGF in cultured cardiomyocytes in both time- and dose-dependent manners (Figure 5C). EPO also upregulated the levels of angiopoietin-1 (*Ang-1*) mRNA in cardiomyocytes, as evidenced by quantitative RT-PCR (qRT-PCR) (Figure 5D). Proliferation and tube formation of HUVEC induced by the conditioned medium from EPO-treated cardiomyocytes were significantly suppressed by a VEGF-specific inhibitor (CBO-P11) or an anti–Ang-1 antibody (Figure 5, A and B). Additionally, when VEGF was knocked down in cardiomyocytes using siRNA, the EPO-induced proliferation of HUVECs was also suppressed (Supplemental Figure 4A). These results suggest that VEGF and Ang-1 secreted from cardiomyocytes mediate the EPO-induced angiogenic response.

Consistent with the in vitro results, EPO treatment markedly increased the levels of VEGF and Ang-1 proteins and *Ang-1* mRNA in the heart after MI (Figure 5, E–G). To determine the role of EPO-mediated VEGF expression in vivo, we injected an adenoviral vector encoding a soluble form of Flt-1, an inhibitor of VEGF, into the thigh muscles of WT mice 4 days before and 3 days after MI. The beneficial effects of EPO on infarcted hearts, including increased vessel number, reduced infarct size, and improved cardiac function, were all abolished by VEGF inhibition (Figure 6), suggesting that VEGF secreted from cardiomyocytes plays a critical role in the cardioprotective effects of EPO against MI.

Shh is a critical mediator of the angiogenic effects of EPO. We further investigated how EPO increases angiogenic cytokine levels in infarcted hearts. Since Akt and ERK, which are activated by EPO, have been reported to regulate VEGF expression (19, 20), we first determined whether EPO increased expression levels of VEGF by activating these kinases in cardiomyocytes. Although both Akt and ERK were activated by EPO in cultured cardiomyocytes, activation levels were not so high as compared with other growth factors such as insulin (Supplemental Figure 2B and data not shown). Since EPO-induced upregulation of VEGF was so robust, we hypothesized that other mitogens mediate the EPO-induced upregulation of VEGF. It has recently been reported that carbamylated EPO (CEPO) promotes neural progenitor cell proliferation and their differentiation into neurons through an upregulation of Shh expression (21). Shh, a critical regulator of patterning and growth in various tissues during embryogenesis, has been reported to show angiogenic effects in infarcted hearts (22, 23). We thus examined the involvement of Shh signaling in EPO-induced cardioprotection.

To determine whether EPO upregulates Shh expression in cardiomyocytes, we first examined the levels of Shh in cultured cardiomyocytes. Both EPO and CEPO induced a marked accumulation of the biologically active, aminoterminal fragment of Shh

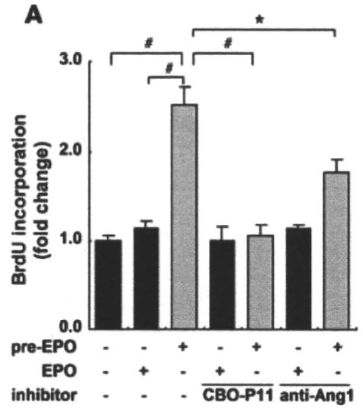

Figure 5

EPO upregulates angiogenic cytokine levels in cardiomyocytes and infarcted heart. (**A**) Endothelial cell proliferation assay using BrdU incorporation. Cardiomyocytes were pretreated with EPO (10 U/ml) or saline for 48 hours. HUVECs were treated with EPO-pretreated conditioned medium (pre-EPO) or saline-pretreated medium with EPO (EPO). Specific inhibitors of VEGF (CBO-P11) and Ang-1 (anti–Ang-1 antibody) were added to the culture medium as indicated. Data from a representative experiment are shown ($n = 5$ per condition). $^{*}P < 0.05$; $^{\#}P < 0.01$. (**B**) Tube formation assay. Quantification of tube length in HUVECs cultured with the conditioned medium was described in **A**. Data from a representative experiment are shown ($n = 3$ per condition). (**C**) Western blotting and quantification of VEGF levels from cultured cardiomyocytes treated with EPO. Time (at dose of 100 U/ml EPO) and dose (treated for 48 hours) dependency are shown ($n = 3$). $^{*}P < 0.05$ versus control. (**D**) qRT-PCR analysis of *Ang-1* mRNA from cultured cardiomyocytes treated with EPO ($n = 4$). Shown are levels of VEGF protein (**E**), Ang-1 mRNA (**F**), and protein (**G**) in the heart after MI. Representative Western blots and quantification are shown. WT mice were subjected to MI and treated with EPO or saline (control) ($n = 4$–5 for each condition).

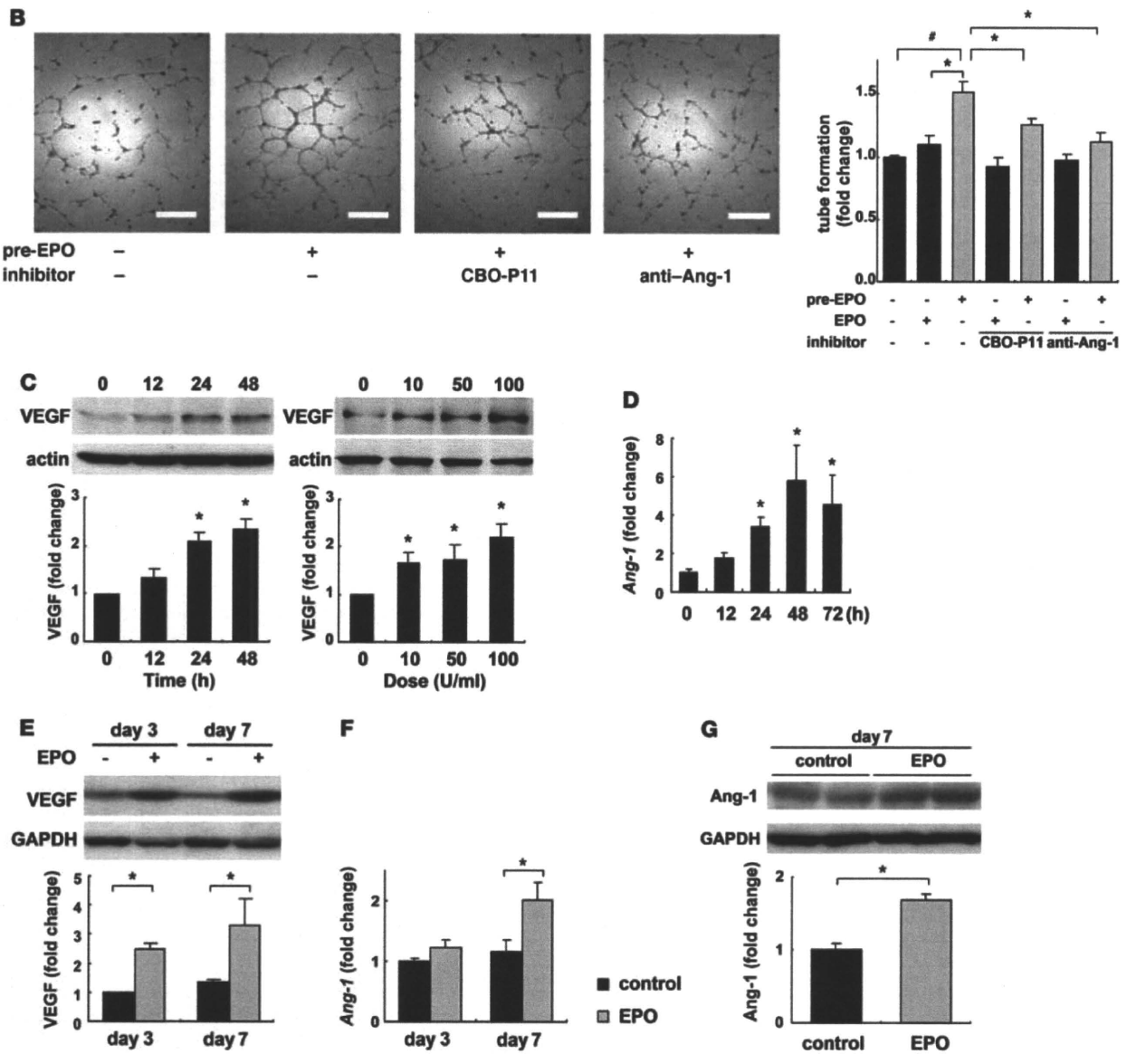

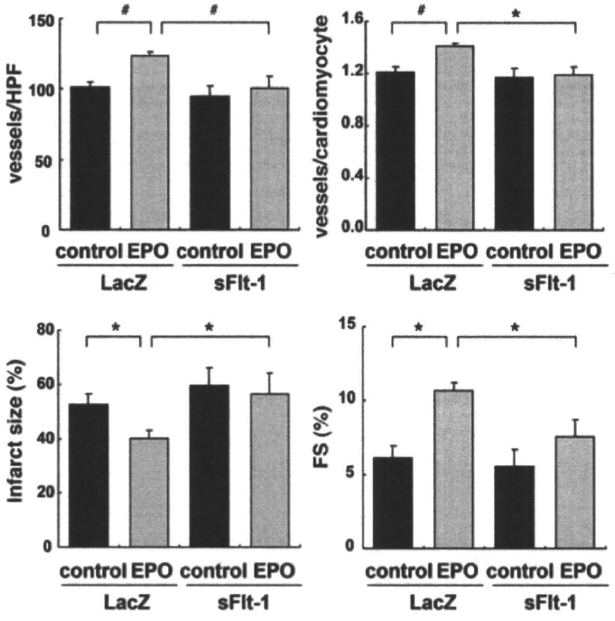

Figure 6

VEGF is essential for the angiogenic and cardioprotective effects of EPO. WT mice were injected with adenoviral vectors encoding soluble Flt-1 (sFlt-1) or LacZ, subjected to MI, and treated with EPO or saline (control). Echocardiographic analysis and immunohistochemical staining were then performed ($n = 8$). $^*P < 0.05$; $^\#P < 0.01$.

(Shh-N) in cardiomyocytes but not in cardiac fibroblasts 48 hours after treatment (Figure 7A), and Shh-N was abundantly secreted from EPO-treated cardiomyocytes into the culture medium (Figure 7B). Immunocytochemical analysis demonstrated that EPO induced the accumulation of Shh in α-sarcomeric actinin–positive cardiomyocytes but not in vimentin-positive cardiac fibroblasts (Figure 7C). In addition, EPO treatment significantly upregulated the levels of *Shh* mRNA in cardiomyocytes (Figure 7D).

We next determined whether Shh augmented angiogenic cytokine levels in cultured cardiomyocytes. Addition of recombinant murine Shh-N peptide (rmShh) increased the mRNA levels of the downstream target genes *Ptch1* and *Gli1* in cardiomyocytes in a dose-dependent manner (Figure 7E). rmShh also increased the levels of VEGF protein and *Ang-1* mRNA in cardiomyocytes as well as the concentration of VEGF protein in the culture medium (Figure 7, E and F). These changes were blocked by cyclopamine, a specific inhibitor of Shh signaling (Figure 7, E and F).

Cyclopamine treatment also significantly inhibited the EPO-induced increases in the levels of VEGF protein and *Ang-1* mRNA (Figure 8, A and B). Moreover, cyclopamine significantly inhibited the proliferation of HUVEC induced by conditioned medium from cardiomyocytes pretreated with EPO (Figure 8C). Consistently, knockdown of Shh in cardiomyocytes also inhibited the EPO-induced proliferation of HUVEC (Supplemental Figure 4B), indicating that EPO induces expression of angiogenic cytokines by activating Shh signaling in cardiomyocytes.

On the other hand, the EPO-induced inhibition of cardiomyocyte apoptosis 24 hours after exposure to H_2O_2 was not affected by cyclopamine (Figure 8D), suggesting that EPO shows its antiapoptotic effects on cardiomyocytes through a Shh-independent pathway.

Cardiomyocyte-specific Shh deletion abolishes EPO-induced cardioprotection. We next determined the role of Shh signaling in EPO-induced cardioprotection in vivo. The expression levels of Shh and Patched were increased in infarcted hearts (Figure 9A), as previously reported (23). Notably, expression levels of Shh and Patched protein were higher in infarcted hearts treated with EPO than in those treated with saline (Figure 9A), indicating that EPO activates Shh signaling in infarcted hearts. Meanwhile, there were no differences in the expression levels of Shh protein in the infarcted hearts of WT and RES mice, suggesting that endogenous EPO signaling is not associated with the upregulation of Shh in the infarcted hearts (Supplemental Figure 5).

Systemic deletion of Shh has been reported to result in cardiovascular defects in mice (24). To elucidate the roles of EPO-induced activation of Shh signaling pathways in infarcted hearts, we employed Shh-MerCre mice in which Shh is deleted only in cardiomyocytes following tamoxifen treatment. We crossed $Shh^{floxed/floxed}$ mice (25) with the transgenic mice in which a transgene encoding Cre recombinase was fused to the mutated estrogen receptor domains (MerCreMer) driven by the cardiomyocyte specific α-myosin heavy chain (α-MHC) promoter (26), and then produced the MHC-MerCreMer; $Shh^{floxed/floxed}$ mutant (Shh-MerCre) mice. After tamoxifen treatment, we confirmed that EPO-induced increases in the expression levels of Shh protein were significantly attenuated in the infarcted hearts of Shh-MerCre mice (Figure 9B). Under basal conditions at 7 days after tamoxifen treatment and at 14 days after MI, there were no significant differences in LV function or the number of vessels and the ratio of vessels to cardiomyocytes among Shh-MerCre mice, $Shh^{floxed/floxed}$ mice, MHC-MerCreMer mice, and WT mice (Figure 9, C and D, and data not shown).

There were no significant differences in LVEDD, FS, and infarct size in the Shh-MerCre mice treated with or without EPO after MI (Figure 9C). EPO did not increase the number of vessels, the ratio of vessels to cardiomyocytes, and the number of α-SMA–positive vessels in Shh-MerCre mice (Figure 9D). EPO treatment also failed to upregulate VEGF protein and *Ang-1* mRNA levels in Shh-MerCre mice (Figure 9, E and F), suggesting that myocardial Shh signaling is critical for the angiogenic and cardioprotective effects of EPO in infarcted hearts.

The role of STAT3 in the mechanism of EPO-induced cardioprotection. We have recently reported that G-CSF prevents LV remodeling after MI through the JAK2/STAT3 pathway in cardiomyocytes (5). To determine whether STAT3 is also involved in cardioprotective effects of EPO, we produced an MI model in transgenic mice that express dominant negative STAT3 in cardiomyocytes under the control of the α-MHC promoter (dnSTAT3-Tg). In dnSTAT3-Tg mice, the EPO treatment reduced infarct size and ameliorated LV dysfunction and remodeling at 14 days after MI by the same degree as WT mice (Supplemental Figure 6A). Overexpression of dnSTAT3 had no effects on EPO-induced prevention of H_2O_2-induced apoptotic death in cardiomyocytes (Supplemental Figure 6B), indicating that STAT3 is not involved in the mechanism of EPO-induced cardioprotective effects after MI.

Discussion

In the present study, we elucidated what we believe are novel mechanisms underlying the EPO-mediated inhibition of cardiac remodeling after MI. EPO enhanced the expression of angiogenic cytokines such as VEGF and Ang-1 in cultured cardiomyocytes and infarcted hearts, which, in turn, induced the proliferation of vas-

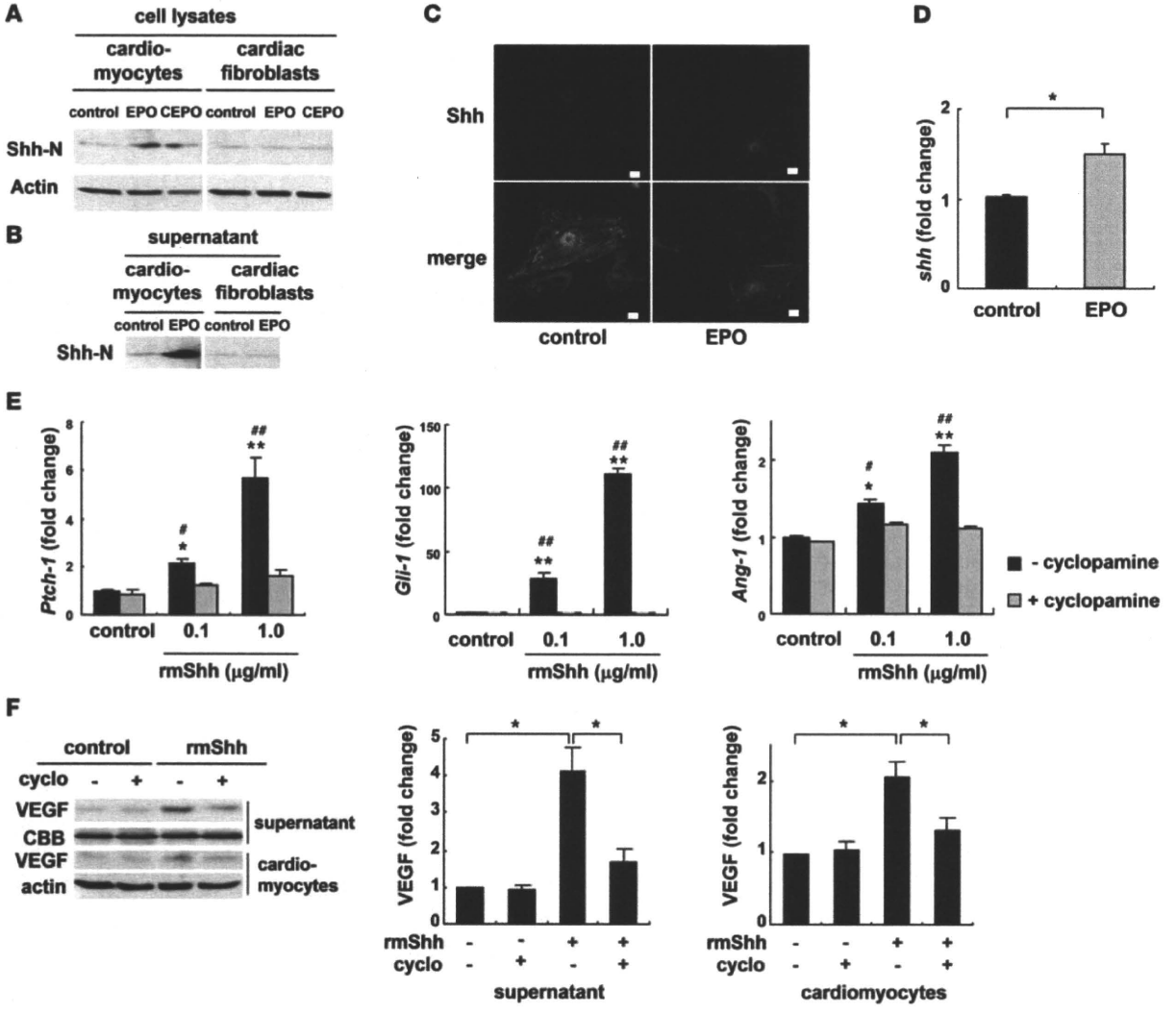

Figure 7

EPO upregulates expression levels of Shh. Western blotting of Shh in cultured neonatal rat cardiomyocytes and cardiac fibroblasts (**A**) and in the culture supernatants (**B**). Cells were treated with EPO (100 U/ml) or CEPO (100 U/ml) for 48 hours. Shh-N represents the aminoterminal domain of Shh, which is a biologically active form of Shh. (**C**) Immunocytochemical staining for Shh (red), α-sarcomeric actinin (green), and vimentin (blue). Cardiomyocytes and cardiac fibroblasts were cocultured with or without EPO for 48 hours. EPO induced the cytoplasmic accumulation of Shh in cardiomyocytes but not cardiac fibroblasts. Scale bars: 10 μm. (**D**) qRT-PCR analysis of *Shh* mRNA. Cardiomyocytes were treated with EPO for 24 hours ($n = 5$). $^{*}P < 0.05$. (**E**) qRT-PCR analysis of *Ptch-1*, *Gli-1*, and *Ang-1* mRNA. Cardiomyocytes were treated with rmShh (0.1 or 1.0 μg/ml) for 24 hours ($n = 4$). $^{*}P < 0.05$; $^{**}P < 0.01$ versus control. $^{\#}P < 0.05$; $^{\#\#}P < 0.01$ versus rmShh and cyclopamine (5 μM) treatment. (**F**) Western blotting of VEGF. Cardiomyocytes were treated with rmShh (1.0 μg/ml) for 48 hours. Cyclopamine (cyclo) was administered 15 minutes before rmShh treatment. Representative Western blots and quantification of the bands are shown ($n = 4$).

cular endothelial cells and angiogenesis. EPO also increased Shh levels in cardiomyocytes, and the various effects evoked by EPO were attenuated by inhibiting Shh signaling (Figure 9G).

We found that EPO promoted angiogenesis by upregulating the expression of VEGF and Ang-1. VEGF is a key molecule that initiates proliferation and migration of endothelial cells and promotes the formation of new vessels, whereas chronic VEGF overexpression in mice has been reported to produce numerous small vessels lacking functional layers (27). Ang-1 induces recruitment of smooth muscle cells to primitive vessels consisting of endothelial cells (27–29). Therefore, our results suggest that EPO treatment might be a better approach to creating stable and functional vessels in infarcted myocardium than the treatment with single angiogenic cytokine. Inhibition of angiogenesis by using the inhibitor of VEGF significantly attenuated the protective effects of EPO, such as the reduction of infarct size and improvement of LV function after MI. Since sufficient coronary perfusion resulting from angiogenesis can prevent cardiomyocyte apoptosis and improve contractile function (30, 31), angiogenic effects as well as direct antiapoptotic effects of EPO might protect the heart after MI. In this study, EPO did not enhance the homing of bone marrow–derived cells in damaged hearts, although EPO induced

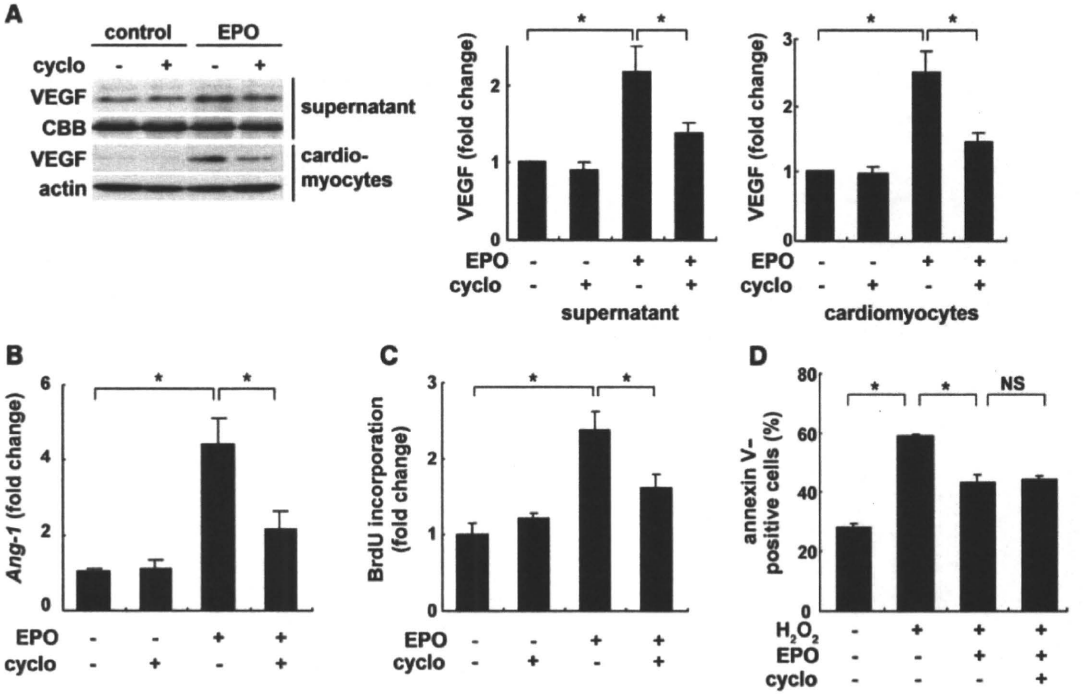

Figure 8

Shh is a critical mediator of the angiogenic effects of EPO in vitro. The expression levels of VEGF protein (**A**) and *Ang-1* mRNA (**B**). Cardiomyocytes were treated with EPO for 48 hours. Cyclopamine (5 μM) was added before EPO treatment. Quantification of the bands is shown ($n = 4$). *$P < 0.05$. (**C**) HUVEC proliferation assay. HUVECs were treated with cardiomyocyte-conditioned medium. Cyclopamine was added before EPO treatment. $n = 5$ per condition. (**D**) Detection of apoptosis using Cy3-labeled annexin V. Quantitative analysis is shown ($n = 6$).

mobilization of bone marrow cells including EPCs from bone marrow into peripheral circulation. It was previously reported that intramyocardial gene transfer of Shh enhanced angiogenesis by bone marrow–derived endothelial cells (23). Although reasons for the different results are not clear at present, the discrepancy may come from expression levels of Shh. Expression levels of Shh produced by intramyocardial gene transfer might be much higher than those induced by subcutaneous injection of EPO, and mode of actions of Shh (i.e., autocrine, paracrine, and endocrine) may be dependent on the expression levels of Shh.

EPO upregulated expression of Shh in cardiomyocytes, which played a critical role in protection of the heart after MI by increasing angiogenic cytokine production. In infarcted hearts, expression levels of Shh and its downstream target Patched have been reported to be increased (23), and Shh has been shown to produce robust angiogenic effects (22, 23). A recent study has demonstrated that cardiomyocyte-specific deletion of *Smoothened*, an essential component of Shh signaling, reduces the expression of angiogenic genes and the number of coronary vessels, resulting in cardiomyocyte apoptosis and cardiac dysfunction, and that vascular smooth muscle cell–specific deletion of *Smoothened* does not affect angiogenesis and cardiac function (32). These results and observations suggest that Shh upregulated by EPO in cardiomyocytes acts on cardiomyocytes themselves in an autocrine manner and increases production of angiogenic cytokines. There were no significant differences in size and function of LV and infarct size among the Shh-MerCre mice, $Shh^{floxed/floxed}$ mice, and MHC-MerCreMer mice without EPO after MI. It has been demonstrated that hedgehog, which is produced mainly by fibroblasts, is critical for maintenance and survival of the coronary vasculature in the adult heart and that the inhibition of endogenous hedgehog by anti-Shh antibody deteriorated cardiac function and induced enlargement of infarct area in the post-MI hearts (32). The discrepancy may come from the different cells of Shh inhibition. Secretion of Shh from other cells including fibroblasts was not inhibited in the cardiomyocyte-specific Shh-deleted mice (Shh-MerCre mice). In neural stem cells, Shh expression is induced via the Notch receptor–mediated activation of cytoplasmic signaling molecules, including Akt, STAT3, and mammalian target of rapamycin (33). Furthermore, it has been also reported that *Shh* is a target gene of NF-κB in mice (34). EPO is known to activate several signaling pathways, including Akt, STAT, and NF-κB in various tissues (19, 35). Further studies are needed to clarify the signaling cascade by which EPO upregulates Shh expression in cardiomyocytes.

We previously demonstrated that angiogenesis promotes cardiac hypertrophy in mice during the early phase of pressure overload (30). We do not know why EPO did not induce cardiomyocyte hypertrophy in this study, but there is a possibility that MI itself induces cardiac and cardiomyocyte hypertrophy via increased wall stress, and EPO-induced reduction of infarct size might reduce the wall stress, resulting in prevention of cardiac and cardiomyocyte hypertrophy even with enhanced angiogenesis.

In conclusion, EPO prevented LV remodeling after MI through Shh. We have reported that G-CSF inhibits cardiomyocyte apoptosis by activating the JAK2/STAT3 pathway in cardio-

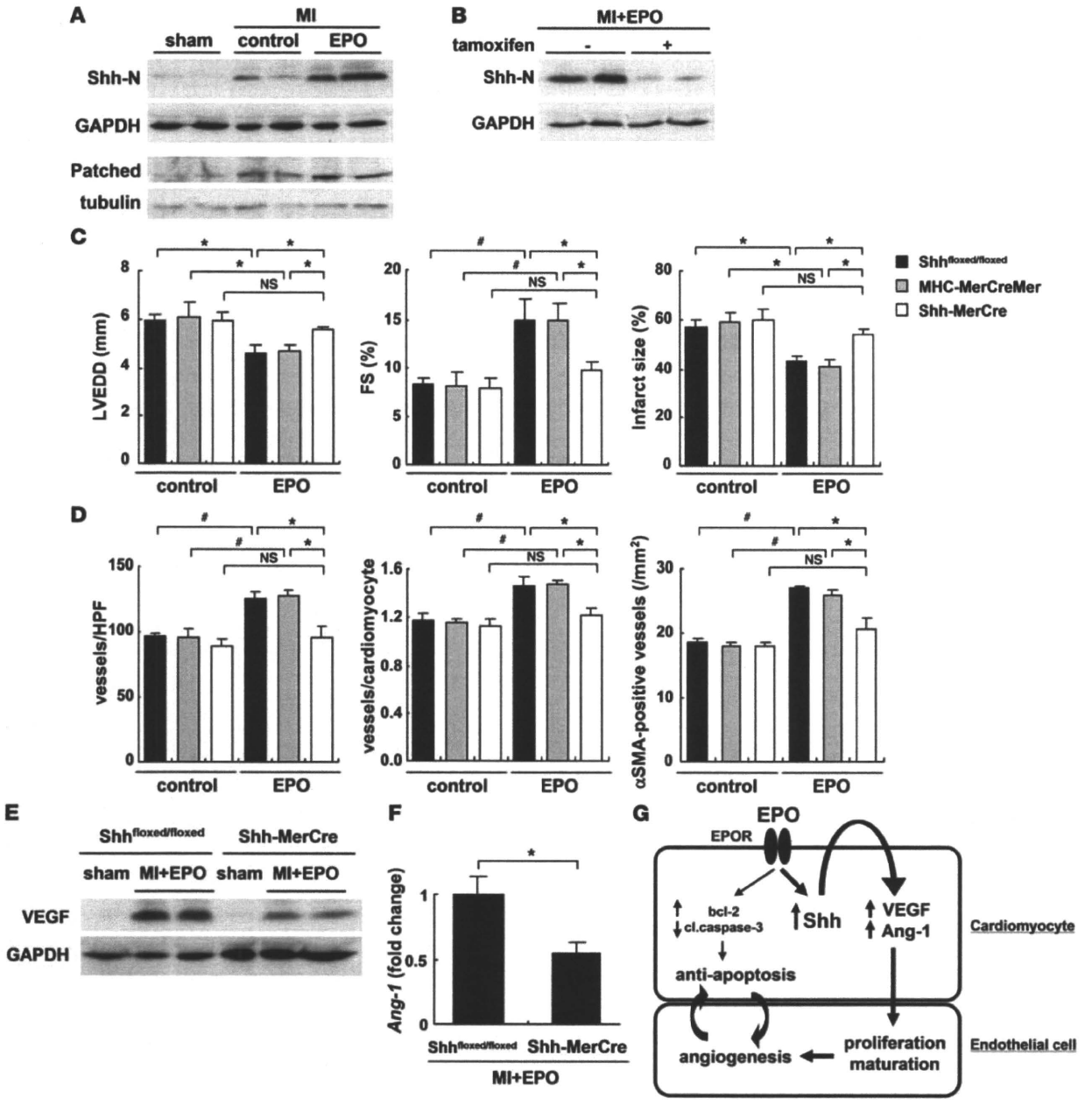

Figure 9

Cardiomyocyte-specific Shh deletion abolishes EPO-induced cardioprotection. (**A**) Activation of Shh signaling after MI and EPO treatment. Hearts were treated with EPO or saline (control) and harvested 4 days (for Shh-N) or 7 days (for Patched) after MI ($n = 4$ for each). (**B**) Western blotting of Shh-N in the infarcted hearts from Shh-MerCre mice treated with or without tamoxifen. Mice were subjected to MI, treated with EPO, and sacrificed 4 days after MI ($n = 4$ for each condition). We measured LVEDD, FS, infarct size (**C**), the number of vessels, the ratio of vessels to cardiomyocyte, and the number of α-SMA–positive vessels (**D**) 14 days after MI ($n = 8$–14). $^{*}P < 0.05$; $^{\#}P < 0.01$. (**E** and **F**) Western blotting of VEGF and qRT-PCR analysis of *Ang-1* mRNA in the heart 7 days after MI. All mice were treated with EPO ($n = 5$). $^{*}P < 0.05$. (**G**) Proposed mechanism underlying the cardioprotective effects of EPO during MI. The mechanisms denoted by the thicker lines are thought to be particularly important.

myocytes, leading to reduced LV remodeling (5). EPO prevented cardiomyocyte apoptosis and protected the heart via the JAK2/STAT3-independent mechanisms, presenting the possibility that administration of the 2 cytokines synergistically protects the heart after MI.

Methods

Animals. All experimental procedures were performed according to the guidelines established by Chiba University for experiments in animals, and all protocols were approved by our institutional review board. Male (C57BL/6 background, 10- to 12-week-old) mice were used in this study.

Shh$^{floxed/floxed}$ mice were purchased from Jackson Laboratory. We injected each mouse with 8 mg/kg of tamoxifen (Sigma-Aldrich) for 12 consecutive days and produced MI at 7 days after tamoxifen treatment. Because EPOR-null mice are embryonic lethal due to severe anemia, we prepared RES mice expressing EPOR exclusively in the hematopoietic lineage, which were established as described previously (15). EPOR expression is limited to the erythroid lineage cells in the RES mice. The RES mice develop normally and are fertile. GFP transgenic mice were purchased from SLC. Generation and genotyping of dnSTAT3-Tg mice have been previously described (36). Age- and sex-matched WT mice (C57BL/6; SLC) were used as controls. RES mice were provided by M. Yamamoto (Tohoku University School of Medicine, Miyagi, Japan).

Induction of MI and treatment. Mice were anesthetized by intraperitoneal injection of pentobarbital (50 mg/kg) and artificially ventilated with a respirator. Mice were subjected to ligation of the left anterior descending artery or to sham operation as described previously (4). Sham operation was performed by cutting pericardium. EPO (Chugai Pharmaceutical) or the same volume of saline was administered subcutaneously.

Echocardiography. Transthoracic echocardiography was performed with a VisualSonics (Vevo 660; VisualSonics Inc.) equipped with a 25-MHz imaging transducer. Mice were kept awake without anesthesia during the echocardiographic examination to minimize data deviation, and heart rate was approximately 550–650 bpm in all mice.

Histology. Hearts fixed in 10% formalin were embedded in paraffin and sectioned at 4-μm thickness for Masson trichrome staining. Tissue hypoxia was evaluated using the Hypoxyprobe (Chemicon) according to the manufacture's instructions. Fixed frozen sections of the heart samples were immunohistochemically stained by using primary antibodies to PECAM (Pharmingen), dystrophin (Novocastra Laboratories), α-SMA (DAKO), and Mac3 (BD Biosciences). The ischemic area that indicates infarct and border area was measured. For measurement of the cross-sectional area of cardiomyocytes, 50 randomly selected cardiomyocytes in a LV cross-section were measured by tracing dystrophin immunostaining. These measurements were performed with NIH ImageJ software. The samples were stained with Hoechst 33258 (1 μg/ml) or TO-PRO-3 (Molecular Probes Inc.). Immunofluorescence was visualized by laser confocal microscopy (Radiance 2000; Bio-Rad Laboratories).

Bone marrow transplantation. Bone marrow cells were isolated from 8-week-old transgenic mice systemically expressing GFP or WT mice. Bone marrow cells (5×10^7 cells) suspended in 100 μl of PBS containing 3% FBS were injected intravenously into irradiated WT mice or RES mice. A flow cytometric analysis revealed that more 97% of bone marrow cells were derived from donor cells at 6 weeks after bone marrow transplantation.

Flow cytometry. Circulating EPCs derived from bone marrow were detected by flow cytometry using CD34/Flk-1 double labeling. Mice subjected to MI or sham operation were treated with EPO or saline for 3 days subsequent to the operation. Then the mice were sacrificed to collect peripheral blood. The nucleated cells were incubated with FITC-conjugated anti-CD34 monoclonal antibody and PE-conjugated anti-Flk-1 antibody (VEGFR2/KDR; BD Biosciences) for 60 minutes on ice and washed with PBS supplemented with 3% FBS. The labeled nucleated cells were analyzed by the EPICS ALTRA flow cytometer using EXPO32 software (Beckman Coulter).

Western blot analysis. Western blot analysis was performed as described previously (30). Briefly, the infarcted hearts were separated into 2 parts consisting of the ischemic and viable regions. Proteins extracted from the ischemic regions of the infarcted hearts of mice were subjected to SDS-PAGE and then transferred onto polyvinylidene difluoride membranes (GE Healthcare). The membranes were probed using a primary antibody against, Shh-N (5E1; Developmental Studies Hybridoma Bank), VEGF, Patched, GAPDH (Santa Cruz Biotechnology Inc.), Ang-1 (Rockland). and α-tubulin (Sigma-Aldrich). For in vitro study, primary antibodies against Shh, Akt, Bcl-2 (Santa Cruz Biotechnology Inc.), VEGF for rat (R&D systems), phospho-Akt, phospho-ERK, cleaved caspase-3 (Cell Signaling), ERK (Invitrogen), and actin (Sigma-Aldrich) were used. The ECL-plus system (GE healthcare) was used for detection. Coomassie Brilliant Blue (Wako Pure Chemical Industries) was used for staining total protein blot with culture medium supernatant of cardiomyocytes.

In vivo gene transfer. Soluble Flt-1 is known to bind to VEGF, thereby acting on as an inhibitor for VEGF (37). We injected an adenoviral vector encoding the murine soluble *Flt-1* gene (10^9 pfu; Invitrogen) into thigh muscles of mice at 4 days before MI and 3 days after MI. Adenoviral vector encoding LacZ (10^9 PFU) was used as control.

Cell culture. Cardiomyocytes prepared from ventricles of 1-day-old Wistar rats were plated onto 35-mm plastic culture dishes at a concentration of 1×10^5 cells/cm^2 and cultured in DMEM supplemented with 10% FBS at 37°C in a mixture of 95% air and 5% CO_2. The culture medium was changed to serum-free DMEM 24 hours before stimulation. rmShh peptide was purchased from R&D Systems. The plasmid of a truncated form of human EPOR was from Y. Nakamura (RIKEN BioResource Center, Tsukuba, Ibaraki, Japan) (38). Adenoviral vector of truncated EPOR was created using AdEasy Vector System (Qbiogene). Adenoviral vector of dnSTAT3 was a gift from K. Yamauchi-Takihara (Osaka University, Osaka, Japan) (36). siRNA targeting VEGF, Shh, and negative control RNA (Invitrogen) were introduced into rat cardiomyocytes by using Lipofectamine RNAiMAX (Invitrogen) according to the manufacturer's instructions. For immunocytochemical staining, cardiomyocytes and cardiac fibroblasts were cocultured with or without EPO for 48 hours, fixed in 4% paraformaldehyde, and stained with primary antibodies to Shh (Santa Cruz Biotechnology Inc.), α-sarcomeric actinin (Sigma-Aldrich), and vimentin (Progen).

qRT-PCR. qRT-PCR analysis was performed as described previously (39). Total RNA was extracted from sample using the RNeasy kit (QIAGEN). We used 2.5 μg of total RNA to generate cDNA using the Super Script VILO cDNA synthesis kit (Invitrogen). qRT-PCR was carried out on a LightCycler system (Roche) using probes from Universal Probe Library (Roche) and the TaqMan Master Mix (Roche). Sequence of primers and the respective Universal Probe Library probes were as follows: *Ang-1*: forward GGAAGATGGAAGCCTGGAT, reverse ACCAGAGGGATTCCCAAAAC, probe #12; *Gapdh*: forward TGTCCGTCGTGGATCTGAC, reverse CCTGCTTCACCACCTTCTTG, probe #80, each for mouse; *Shh*: forward GAATCCAAAGCTCGCATCC, reverse CAGGTGCACTGTGGCTGAT, probe #38; *Ang-1*: forward GGAAGCCTAGATTTCCAGAGG, reverse ACCAGAGGGATTCCCAAAAC, probe #12; *Ptch-1*: forward CAAAGCTGACTACATGCCAGA, reverse GCGTACTCTATGGGCTCTGC, probe #64, *Gli-1*: forward GGAAGAGAGCAGACTGACTGTG, reverse GGGGAGTGGTCACTGCTG, probe #1; and *Gapdh*: forward AATGTATCCGTTGTGGATCTGA, reverse GCTTCACCACCTTCTTGATGT, probe #80, each for rat. Relative expression of target genes was calculated with the comparative CT method. Each sample was run in duplicate, and the results were systematically normalized using *Gapdh*.

Apoptosis analysis. Frozen sections of the heart samples and cultured cardiomyocytes fixed by 4% paraformaldehyde were subjected to TUNEL staining using a commercially available kit (In Situ Apoptosis Detection Kit; Takara Biomedicals) as directed by manufacturer. Annexin V-Cy3 Apoptosis Detection Kit (BioVision) was used to detect apoptotic cardiomyocytes according to the manufacture's instructions. Cultured cardiomyocytes were serum starved in DMEM with 0.5% FBS and treated with EPO (10 U/ml) or normal saline for 8 hours prior to beginning H_2O_2 (100 μM) treatment. Cyclopamine (40–42) (5 μM), LY294002 (5 μM), and PD98059 (10 μM; Calbiochem) were administered 15 minutes before EPO treatment.